Mass transfer with complex chemical reactions in gas–liquid systems

Vas Bhat, R.D.; Kuipers, J.A.M.; Versteeg, G.F.

Published in:
Chemical Engineering Journal

Publication date:
2000

ELSEVIER

Chemical Engineering Journal 76 (2000) 127–152

Chemical Engineering Journal

www.elsevier.com/locate/cej

Mass transfer with complex chemical reactions in gas–liquid systems: two-step reversible reactions with unit stoichiometric and kinetic orders

R.D. Vas Bhat *, J.A.M. Kuipers, G.F. Versteeg

Department of Chemical Technology, University of Twente, PO Box 217, 7500 AE Enschede, The Netherlands

Received 31 July 1998; received in revised form 6 August 1999; accepted 13 August 1999

Abstract

An absorption model to study gas–liquid mass transfer accompanied by reversible two-step reactions in the liquid phase has been presented. This model has been used to determine mass transfer rates, enhancement factors and concentration profiles over a wide range of process conditions. Although results presented in this paper deal with reactions of unit stoichiometric and kinetic orders only, the model has been prepared for general orders. The effect of reversibility of each individual reaction along with their combined reversibility has been presented over a wide range of Hatta numbers. Influence of species diffusivity has also been considered. It has been shown that for low mobility of the gaseous species, the enhancement by reversible reactions can be higher than the corresponding enhancement obtained assuming the reactions to be irreversible. The presence of solute loading has been found to significantly affect the absorption characteristics of the system. An approximate method to determine infinite enhancement factors for reversible two-step reactions has been presented. The match between numerically predicted results and those obtained from the approximate technique was found to be within 0.05%. Finally, the present model has been validated against a practical system. The absorption of CO_2 in NaOH and bicarbonate solutions in model contactors has been chosen for this purpose. An excellent agreement was observed for a wide range of gas–liquid contact times.

Keywords: Two-step reaction; Gas–liquid system; Mass transfer; Stoichiometry

1. Introduction

Extensive studies into mass transfer accompanied by chemical reactions have been conducted previously. Complex reactions in the liquid phase have played a major role in this research [1]. However, as was indicated in the above mentioned review, very limited attention has been paid to processes involving two-step reactions in the liquid phase. These two-step reactions are classified as those that proceed according to the following reaction stoichiometry:

$$A(g) \rightarrow A(I) \tag{1a}$$

$$A(I) + B(I) \overset{k_{1,1}/k_{1,2}}{\leftrightarrow} C(I) + D(I) \tag{1b}$$

$$B(I) + C(I) \overset{k_{2,1}/k_{2,2}}{\leftrightarrow} E(I) + F(I) \tag{1c}$$

Some well-known two-step systems of importance in gas treatment are the absorption of Cl_2 and SO_2 in caustic solutions and the absorption of CO_2 in NaOH solutions or bicarbonate buffers.

The first known study on gas–liquid mass transfer with two-step reaction was conducted by Brian and Beaverstock [2]. Limited research on this system has been carried out thereafter. A concise review of previous research on the two-step reaction system is presented in Table 1.

2. Theory

2.1. Species transport equations

Two-step reactions may be represented by the stoichiometry given in (1a)–(1c). The numerical model, however, has been prepared to take general stoichiometric and kinetic orders into account. Based on the penetration theory, the unsteady state mass balances can be written as:

$$\frac{\partial A}{\partial t} = D_A \frac{\partial^2 A}{\partial x^2} - R_{A1}, \tag{2a}$$

* Corresponding author. Present address: Unilever Research Vlaardingen, PO Box 114, 3130 AC Vlaardingen, The Netherlands. Tel.: +31-10-460-6019; fax: +31-10-460-5192

E-mail address: rahul.vasbhat@unilever.com (R.D. Vas Bhat)

1385-8947/00/$ – see front matter
PII: S1385-8947(99)00104-7

Table 1
Review of previous literature on two-step reactions

Author(s)	$A + B \leftrightarrow^{k_1} C + D$	$B + C \leftrightarrow^{K_2} E + F$	Mass transfer theory	Solution type	Remarks
Brian and Beaverstock [2]	Irreversible	Irreversible	Film, penetration	Numerical	Equal diffusivities, qualitative effect of diffusivity on enhancement
Ramachandran [5]	Instantaneous, irreversible	Irreversible (1, 1) or (0, 1) order	Film	Exact and approximate	Unequal diffusivities, approximate solution based on Hikita–Asai linearisation
	Fast, irreversible	Irreversible	Film	Approximate	Unequal diffusivities, Hikita–Asai linearisation
Hikita et al. [12]	Instantaneous, reversible	Instantaneous, reversible	Penetration	Exact	Equal diffusivities: K_1, $K_2 \rightarrow \infty$
	Instantaneous, reversible	Instantaneous, reversible	Penetration	Approximate	Unequal diffusivities: K_1, $K_2 \rightarrow \infty$; $K_1/K_2 \rightarrow \infty$
Hikita and Asai [10]	Irreversible	Instantaneous, reversible	Film, penetration	Approximate	Unequal diffusivities
Bhattacharya and Ramachandran [6]	Instantaneous, reversible	Instantaneous, reversible	Film	Exact	Equal diffusivities, no limitation on K_1 and K_2

$$\frac{\partial B}{\partial t} = D_B \frac{\partial^2 B}{\partial x^2} - R_{A1} - R_{A2}, \tag{2b}$$

$$\frac{\partial C}{\partial t} = D_C \frac{\partial^2 C}{\partial x^2} + R_{A1} - R_{A2}, \tag{2c}$$

$$\frac{\partial D}{\partial t} = D_D \frac{\partial^2 D}{\partial x^2} + R_{A1}, \tag{2d}$$

$$\frac{\partial E}{\partial t} = D_E \frac{\partial^2 E}{\partial x^2} + R_{A2}, \tag{2e}$$

$$\frac{\partial F}{\partial t} = D_F \frac{\partial^2 F}{\partial x^2} + R_{A2}, \tag{2f}$$

with reaction rates described by Eqs. (3a) and (3b).

$$R_{A1} = k_{1,1} A^m B^n - k_{1,2} C^p D^q, \tag{3a}$$

$$R_{A2} = k_{2,1} B^r C^s - k_{2,2} E^u F^v. \tag{3b}$$

Reactions in gas–liquid systems can usually be expressed with sufficient accuracy by means of power law kinetics, as given above. However, other kinetic forms, such as the Langmuir–Hinshelwood type can easily be included in the present model. The unsteady state mass balances have been solved with the following initial (Eq. (4a)) and boundary conditions (Eqs. (4b)–(4d)):

Initial:

$$t = 0; \quad x \geq 0 \Rightarrow A = A_0; \quad B = B_0; \quad C = C_0; \quad D = D_0; \quad E = E_0; \quad F = F_0, \tag{4a}$$

Boundary:

$$t > 0; \quad x = 0 \Rightarrow k_G \left(A_G - A_{i,G}\right) = -D_A \left(\frac{\partial A}{\partial x}\right)_{x=0}, \tag{4b}$$

$$t > 0; \quad x = 0 \Rightarrow \left(\frac{\partial B}{\partial x}\right)_{x=0} = \left(\frac{\partial C}{\partial x}\right)_{x=0} = \left(\frac{\partial D}{\partial x}\right)_{x=0} = \left(\frac{\partial E}{\partial x}\right)_{x=0} = \left(\frac{\partial F}{\partial x}\right)_{x=0} = 0, \tag{4c}$$

$$t > 0; \quad x \rightarrow \infty \Rightarrow A = A_0; \quad B = B_0; \quad C = C_0; \quad D = D_0; \quad E = E_0; \quad F = F_0. \tag{4d}$$

For reversible reactions, one always need to consider the bulk equilibrium of all chemical species involved in the reactions. The extent of solute loading is determined by the loading factor, α:

$$A_T = \alpha B_T, \tag{5a}$$

where A_T and B_T are the total bulk concentrations of A and B in all forms:

$$A_T = A_0 + D_0, \tag{5b}$$

$$B_T = B_0 + D_0 + E_0. \tag{5c}$$

For a given bulk concentration of B, the bulk concentrations of all other species can be calculated by means of the equilibrium definitions and mass balances

$$K_1 A_0 B_0 - C_0 D_0 = 0, \tag{5d}$$

$$K_2 B_0 C_0 - E_0 F_0 = 0, \tag{5e}$$

$$D_0 - C_0 - E_0 = 0, \tag{5f}$$

$$E_0 - F_0 = 0, \tag{5g}$$

where K_1 and K_2 are defined as the equilibrium constants for reactions (1b) and (1c), respectively, for the case where all kinetic orders are equal to unity. The equilibrium reactions (5d)–(5g) are sufficient to describe the reaction stoichiometry under consideration. However, for applications to practical systems, it is usually necessary to consider additional equilibria. For example, aqueous equilibria and/or electroneutrality would have to be considered in the case of electrolytic systems.

2.2. Numerical model

The set of partial differential Eqs. (2a)-(2f), subject to initial and boundary conditions Eqs. (4a)-(4d) was solved

Table 2
Program input parameters

Variable	Value	Units
A_i	10	$\mathrm{mol\,m^{-3}}$
B_T	40	$\mathrm{mol\,m^{-3}}$
k_L	10^{-4}–10^{-7}	$\mathrm{m\,s^{-1}}$
$k_{1,1}$	0.25–2.6 × 10^5	$\mathrm{m^3\,mol^{-1}\,s^{-1}}$
K_1	0.01–100	–
K_2	0.01–100	–
K_{R2}	10^{-5}–1	–
α	0.001–0.99	–
D_B	10^{-9}	$\mathrm{m^2\,s^{-1}}$

using a technique similar to that described previously [3]. The numerical code has been implemented in PASCAL.

The set of equilibrium Eqs. (5a)-(5e) were solved separately using a Newton–Raphson algorithm for a given value of B_T, K_1 and K_2 to obtain the initial concentrations of all species at different loading factors. The input variables used in the simulations presented in this paper are given in Table 2. Validation of the numerical code has been reported earlier [4].

3. Effect of reaction reversibility on two-step reactions

On account of the large number of parameters that can be varied in two-step reaction systems, results presented in this paper are limited to reactions with unit stoichiometric and kinetic orders. In order to understand the underlying mass transfer phenomena, the following dimensionless numbers have been used:

The enhancement factor, E_A, is defined as:

$$E_A = \frac{N_A}{k_L\,(A_i - A_0)}, \tag{6a}$$

where N_A is the absorption flux at identical concentration gradient.

The Hatta number, Ha, is based on reaction (1b) and is defined as:

$$\mathrm{Ha} = \frac{\sqrt{k_{1,1} B_0 D_A}}{k_L}. \tag{6b}$$

The Hatta numbers were varied by changing the liquid mass transfer coefficient, k_L, or the kinetic rate constants. The varying parameter in the graph, K_{R2}, is defined as the ratio of the two forward reaction rate constants:

$$K_{R2} = k_{2,1} k_{1,1}. \tag{6c}$$

3.1. Both reactions irreversible

The variation of E_A with Hatta number as a function of K_{R2} is presented in Fig. 1. K_{R2} is varied between two asymptotic values. A $K_{R2} = 0$, indicates that rate of reaction (1c) is negligible as compared to reaction (1b). Conversely, for a $K_{R2} = \infty$, the rate of reaction (1b) is negligible as compared to reaction (1c) so that all C formed is immediately converted to E and F. Overall stoichiometry is identical to Eq. (7). For intermediate values of K_{R2}, enhancement behaviour can be explained on the basis of competition between A and C for reaction with B.

- For low Hatta numbers (typically <10), only reaction (1b) influences mass transfer and the system behaves similar to a single bimolecular irreversible reaction. With an increase in Ha, sufficient intermediate, C is formed by reaction (1b). This results in a competition between A and C for reaction with B. The increased consumption of B by C at higher Hatta numbers reduces the absorption of A, thereby reducing the enhancement factor. At extremely high Ha (Ha > 10^6) both reactions are instantaneous with respect to mass transfer. Consequently, reaction (1b) and reaction (1c) can be added and simplified to:

$$\mathrm{A(l)} + 2\mathrm{B(l)} \rightarrow \mathrm{D(l)} + \mathrm{E(l)} + \mathrm{F(l)} \tag{7}$$

  with an irreversible infinite enhancement factor, $E_{\infty,\mathrm{irr}}$, defined as:

$$E_{\infty,\mathrm{irr}} = \left(1 + \frac{D_B B_0}{2 D_A A_i}\right)\sqrt{\frac{D_A}{D_B}}. \tag{8}$$

  All reactions, irrespective of K_{R2}, finally converge to the same $E_{\infty,\mathrm{irr}}$.
- With an increase in K_{R2}, the effect of reaction (1c) on the enhancement factor is visible at increasingly lower Hatta numbers. Its effect on the overall enhancement is observed even before reaction (1b) can reach its infinite value, so that the intermediate asymptotic enhancement factor ($E_{\infty 1}$) reduces with an increase in K_{R2}. At even higher K_{R2} ($K_{R2} > 10$), reaction (1c) becomes instantaneous even before reaction (1b) does so that the enhancement curve tends to the final infinite enhancement factor (E_∞) without reaching its asymptotic value and the peak in enhancement disappears.

A similar variation in enhancement with the Hatta number was observed by Brian and Beaverstock [2]. The model presented in the present study was found to be in good agreement to their results (max. deviation <1.5%).

Ramachandran [5] presented approximate solutions for the case where reaction (1b) was instantaneous. Comparison between the results obtained from the present model and the solutions of Ramachandran [5] showed that maximum deviations occurred when reaction (1c) was in the fast reaction regime (when enhancement drops from $E_{\infty 1}$ to E_∞). In this region, the Hikita–Asai linearisation of the concentration profile of B (that was assumed by Ramachandran) is not valid, which accounts for the deviation from the numerical solution. With a further increase in the Hatta number, the reaction enters the instantaneous reaction regime and the profile of B is linear once again and the difference between approximate and numerical solutions is negligible.

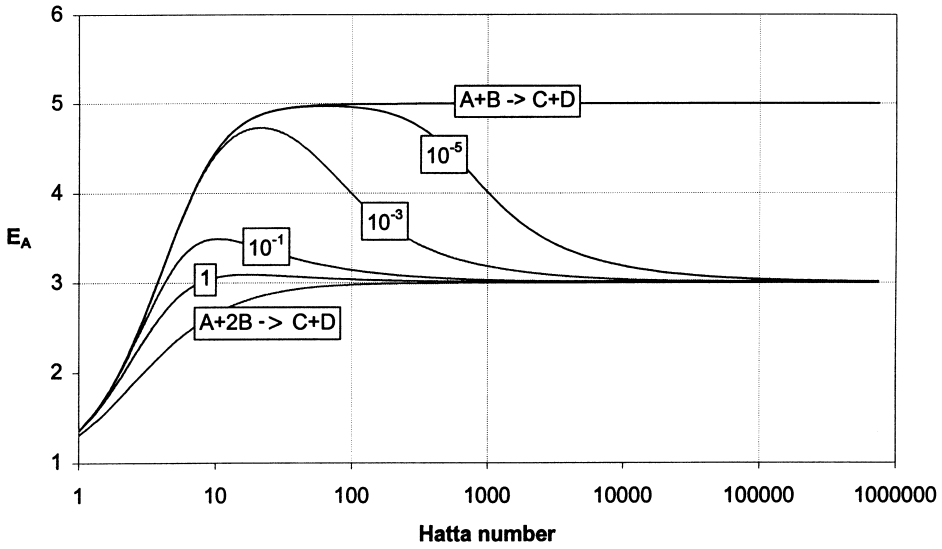

Fig. 1. Effect of K_{R2} on enhancement factor. Both reactions irreversible.

Table 3
Simulation parameters for concentration profiles given in Fig. 2b–e[a]

Case	k_L ($m\,s^{-1}$)	$k_{1,1}$ ($m^3\,mol^{-1}\,s^{-1}$)	Ha (−)	E_A (−)
I	1.10×10^{-6}	2.50×10^{-1}	90.5	4.96
II	9.77×10^{-8}	2.50×10^{-1}	1024	4.01
III	9.77×10^{-8}	3.20×10^{1}	11 585	4.03
IV	9.77×10^{-8}	1.31×10^{5}	7.41×10^{5}	4.99

[a] $K_2 = 100$; $K_{R2} = 10^{-5}$.

3.2. First reaction irreversible, second reaction reversible

The results for the simulation for the above case are given in Fig. 2a for $K_{R2} = 10^{-5}$. The initial part of the curve is similar to a second order irreversible reaction till the curve reaches the intermediate asymptotic enhancement factor. As the Hatta number increases further, reaction (1b) becomes instantaneous with respect to mass transfer and changes in enhancement are now caused by reaction (1c) only.

Reversibility of reaction (1c) first causes the enhancement factor to drop with increasing Hatta number, but enhancement increases once again for very high Hatta numbers. The decrease in enhancement is proportional to the K_2 value and occurs at higher Hatta numbers for a higher value of K_2. The value K_2 does not affect the final infinite enhancement factor, E_∞. In this case, E_∞ is the same as the intermediate asymptotic enhancement factor.

In order to explain the mass transfer behaviour observed in Fig. 2a, concentration profiles (Fig. 2b: Cases I–IV) have been generated at four different Hatta numbers, as indicated in the figure, for a single value of $K_2 = 100$. It is at this value of K_2 that the decrease in enhancement factor is most pronounced. Simulation parameters are presented in Table 3. The profiles for component F are the same as that for E.

- *Case I* (Ha = 90.5): The reaction between A and B (1b) can be regarded as instantaneous as is observed by the formation of a distinct reaction plane in the concentration profile (Fig. 2b). The effect of reaction (1c) is negligible as it is seen from the fact that there is hardly any production of E and F. As a result, at this point, absorption of A is influenced by reaction (1b) only.
- *Case II* (Ha = 1024): The concentration of C is lower than that of D indicating that some of the C produced by reaction (1b) reacts with B via the forward reaction of (1c). This is confirmed because some production of E and F is observed in Fig. 2c. Thus, B reacts via two parallel paths. The competition for B reduces the absorption rate of A and causes the enhancement factor to fall.
- *Case III* (Ha = 11 585): In Case II, the concentration of A is linear until the reaction plane formed with B which means that no reaction of A is occurring in this region. However, in Case III (Fig. 2d), the profile is curved indicating occurrence of reaction in this region. E and F are reverted via reaction (1c) and produce B and C. Since B and A cannot occur simultaneously in this region on account of the instantaneous fast reaction (1b), it immediately reacts with A to form C and D. Thus, there is a combination of reaction (1b) with the backward reaction of (1c). The overall stoichiometry is given by:

$$A(l) + E(l) + F(l) \leftrightarrow 2C(l) + D(l) \quad (1d)$$

Thus, additional absorption of A is taking place due to the mechanism indicated above which causes the enhancement to increase once again. In the second reaction zone observed in the figure, C reacts with B to generate E and F via the forward reaction (1c).

Case IV (Ha = 7.41×10^5): At these high Hatta numbers, the overall reaction (1d) becomes instantaneous and a clear reaction plane between A and components E and F is observed. Since the concentration of E (and F) is the same as B (for the instantaneous case), the absorption rate of A in Case IV is the same as that in Case I resulting in the enhancement factor being restored to its value in Case I.

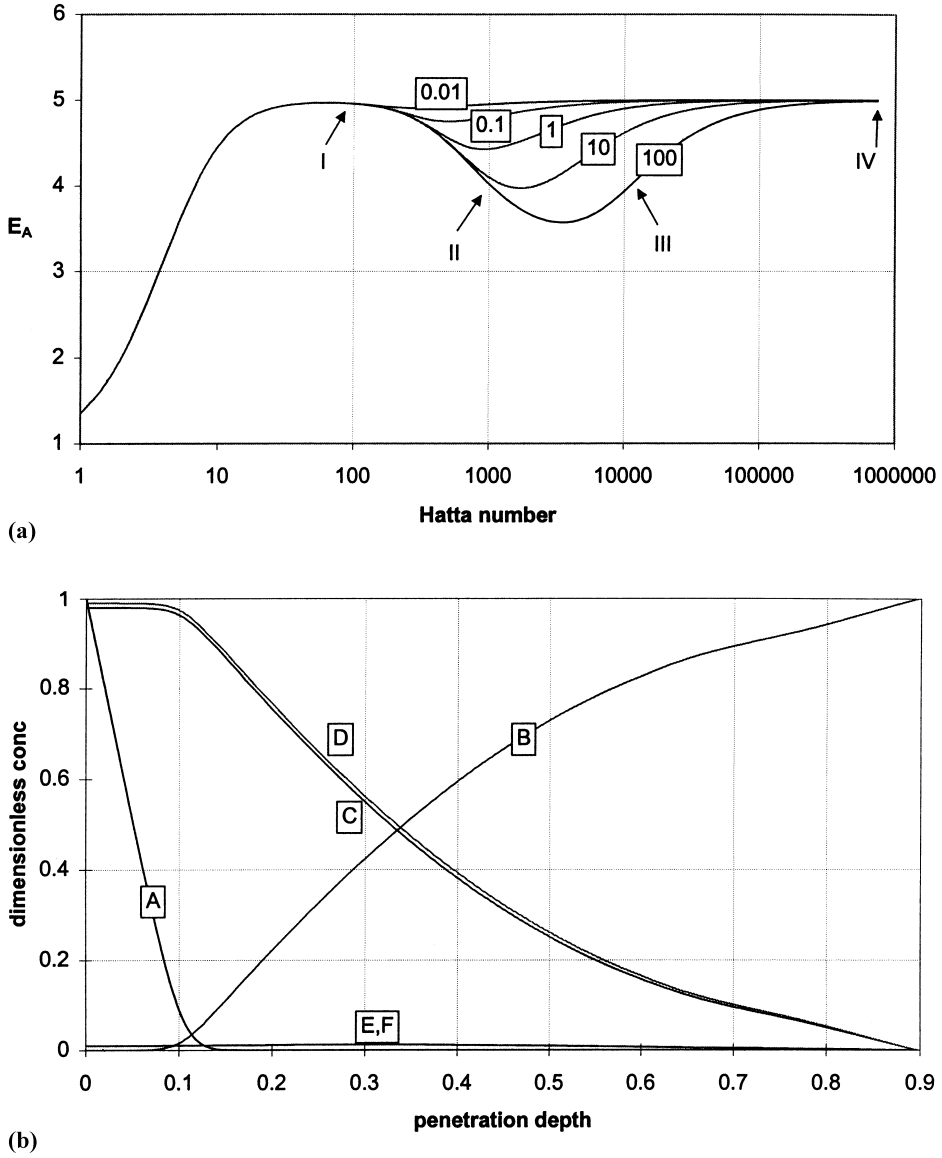

Fig. 2. (a) Two step Irreversible-Reversible reaction. Effect of K_2 on enhancement factor; $K_{R2} = 10^{-5}$. Concentration profiles for Cases I–IV given in Figure 2b to 2e respectively, (b) Case I: Concentration profiles at Ha = 90.5. $K_2 = 100$; $K_{R2} = 10^{-5}$, (c) Case II: Concentration profiles at Ha = 1024. $K_2 = 100$; $K_{R2} = 10^{-5}$. (d) Case III: Concentration profiles at Ha = 11585. $K_2 = 100$; $K_{R2} = 10^{-5}$. (e) Case IV: Concentration profiles at Ha = 7.41×10^5, $K_2 = 100$; $K_{R2} = 10^{-5}$.

3.3. First reaction reversible, second reaction irreversible

The results for the simulation for the above case are presented in Fig. 3 for $K_{R2} = 10^{-5}$. The influence of K_1 on enhancement is characterised as follows:

- K_1 affects the intermediate asymptotic enhancement factor, $E_{\infty 1}$, while the value of E_∞ remains the same irrespective of the value of K_1. In the instantaneous reaction regime the system reduces to reaction (7) with the overall enhancement described by (8).
- K_1 also affects the point at which reaction (1c) starts influencing the overall mass transfer. A higher K_1 results in greater production of C by reaction (1b) resulting in the effect of reaction (1c) being visible at lower Hatta numbers.

For higher values of K_1 (typically $K_1 > 1$), the enhancement factor first rises and then falls to its final value while for lower K_1 values (typically ≤ 1), the approach to infinite enhancement is from below. This is explained by observing the concentration profiles for two extreme values of K_1. The concentration profiles for $K_1 = 100$ are given in Fig. 4a and b while those for $K_1 = 0.01$ are given in Fig. 5a and b, respectively. The corresponding input parameters are given in Table 4.

For $K_1 = 100$, Case I (Fig. 4a), the rate of the forward reaction of (1b) is high causing a large production of C

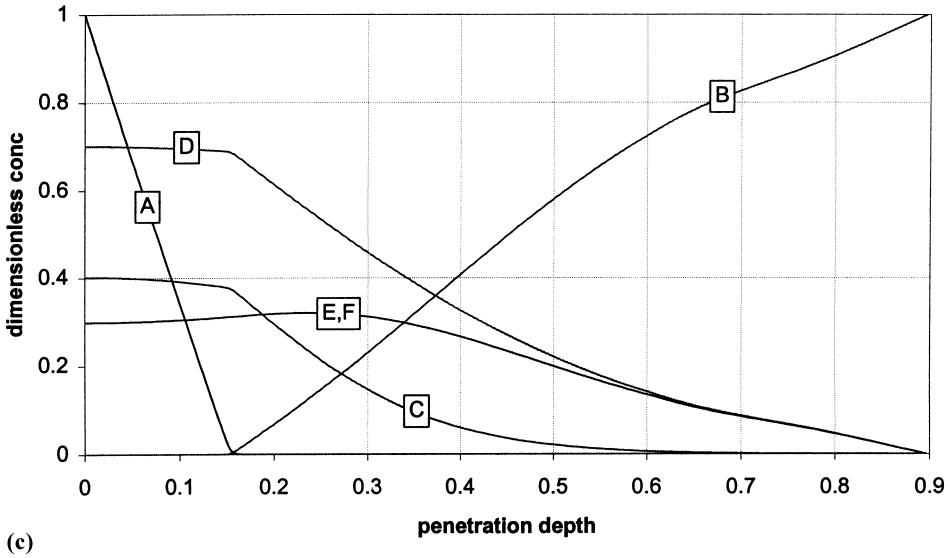

(c)

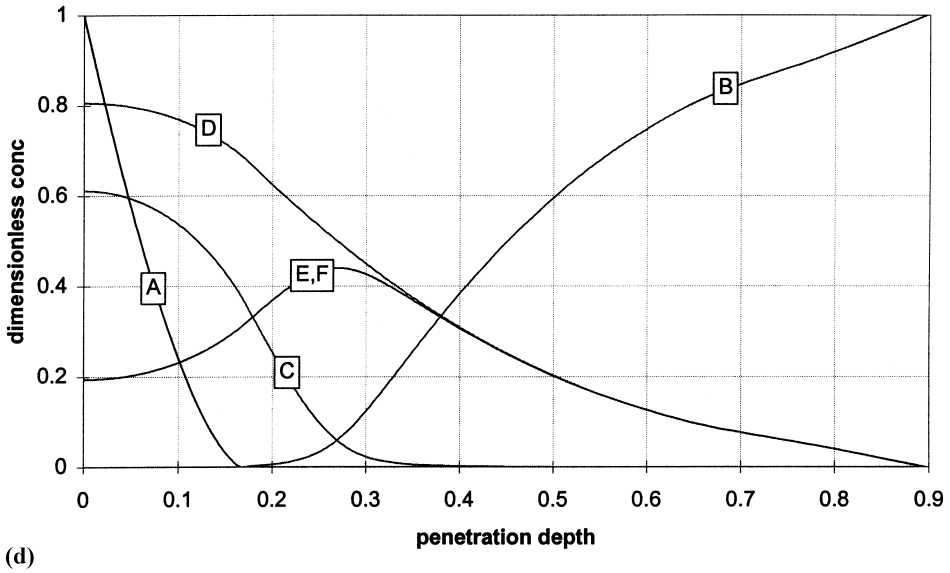

(d)

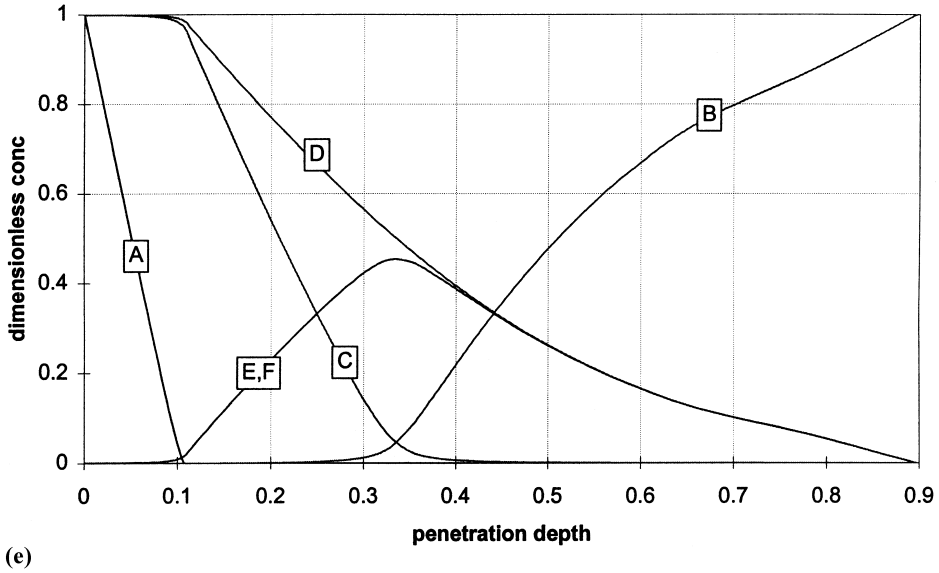

(e)

Fig. 2. (*Continued*).

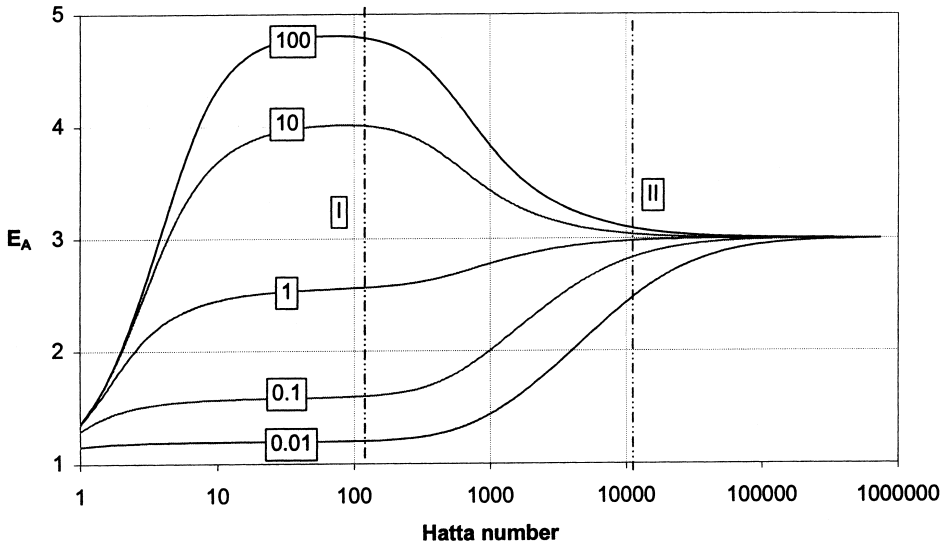

Fig. 3. Two-step Reversible-Irreversible reaction. Effect of K_1 on enhancement; $K_{R2} = 10^{-5}$. Concentration profiles for Cases I–II in Figs. 4a and b ($K_1 = 100$) and Figs. 5a and b ($K_1 = 0.01$).

Table 4
Simulation parameters for concentration profiles given in Fig. 4a and b and Fig. 5a and b[a]

Case	k_L (m s^{-1})	$k_{1,1}$(m^3 mol^{-1} s^{-1})	Ha (−)	E_A	
				$K_1 = 0.01$	$K_1 = 100$
I	7.81×10^{-7}	2.50×10^{-1}	128	1.20	4.78
II	9.77×10^{-8}	3.20×10^{1}	11585	2.49	3.09

[a] $K_{R2} = 10^{-5}$.

(and D), in turn, resulting in a relatively high intermediate asymptotic enhancement factor. With an increase in Hatta number, the present C can react with B (via (1c)). This competition for B is sufficient to reduce the rate of absorption of A via reaction (1b) and reduce enhancement. This is observed in Case II (Fig. 4b) where the average concentration of C is close to zero due to its reaction with B and the reaction plane between A and B is shifted towards the bulk indicating a lower enhancement.

For $K_1 = 0.01$, Case I (Fig. 5a), the low equilibrium constant results in limited formation of C and a low enhancement factor as well. With an increase in Hatta number, C is consumed by B (via (1c)). The reduction in B, however, is not significant enough to reduce the absorption of A. On the contrary, the removal of C from the system shifts the equilibrium of reaction (1b) causing additional absorption of A. The enhancement factor increases and approaches its final value from below (Fig. 5b).

3.4. Both reactions reversible

Typical results for this type of reaction are presented in Fig. 6a and b. The overall effects are a combination of those observed for systems indicated in Sections 3.2 and 3.3.

3.4.1. Effect of K_1

At a fixed value of K_2 (Fig. 6a), some interesting features of the enhancement curve are observed. For $K_1 = 100$, with an increase in the Hatta number, the enhancement factor first goes through a local maximum ($E_{\infty 1}$) and then a local minimum (E_{min}) before approaching the final infinite enhancement factor (E_∞). The local maximum is reached in the absence of reaction (1c) while the decrease in enhancement ($90 < Ha < 2900$) is caused by the competition for B between A and C resulting in a decrease in absorption of A. Beyond this Hatta number ($Ha > 2900$), the enhancement factor increases once again. At these high Hatta numbers, the reaction of E and F with A causes an increased additional absorption of A. The reaction stoichiometry is similar to (1d) with equilibrium constant defined as:

$$K_3 = \frac{C^2D}{AEF} = \frac{CD}{AB} \cdot \frac{BC}{EF} = \frac{K_1}{K_2}. \quad (9)$$

This increase in enhancement observed, ΔE_A, may be defined as :

$$\Delta E_A = E_\infty - E_{min}. \quad (10)$$

Since ΔE_A is caused by reaction (1d), its value would be larger for smaller values of K_2, as seen from (9). Simulations with the present model showed that ΔE_A increased from 2.5% to 4.3% with a reduction in K_2 from 100 to 10 while keeping K_1 fixed at a value of 100.

3.4.2. Effect of K_2

At a fixed value of K_1, K_2 affects the value of the final infinite enhancement factor, E_∞. If the value of $E_{\infty 1}$ is lower than the final infinite enhancement factor for the case where both reactions are irreversible ($E_{\infty,irr}$), then enhancement is increased proportional to K_2 (Fig. 6b). This can be explained

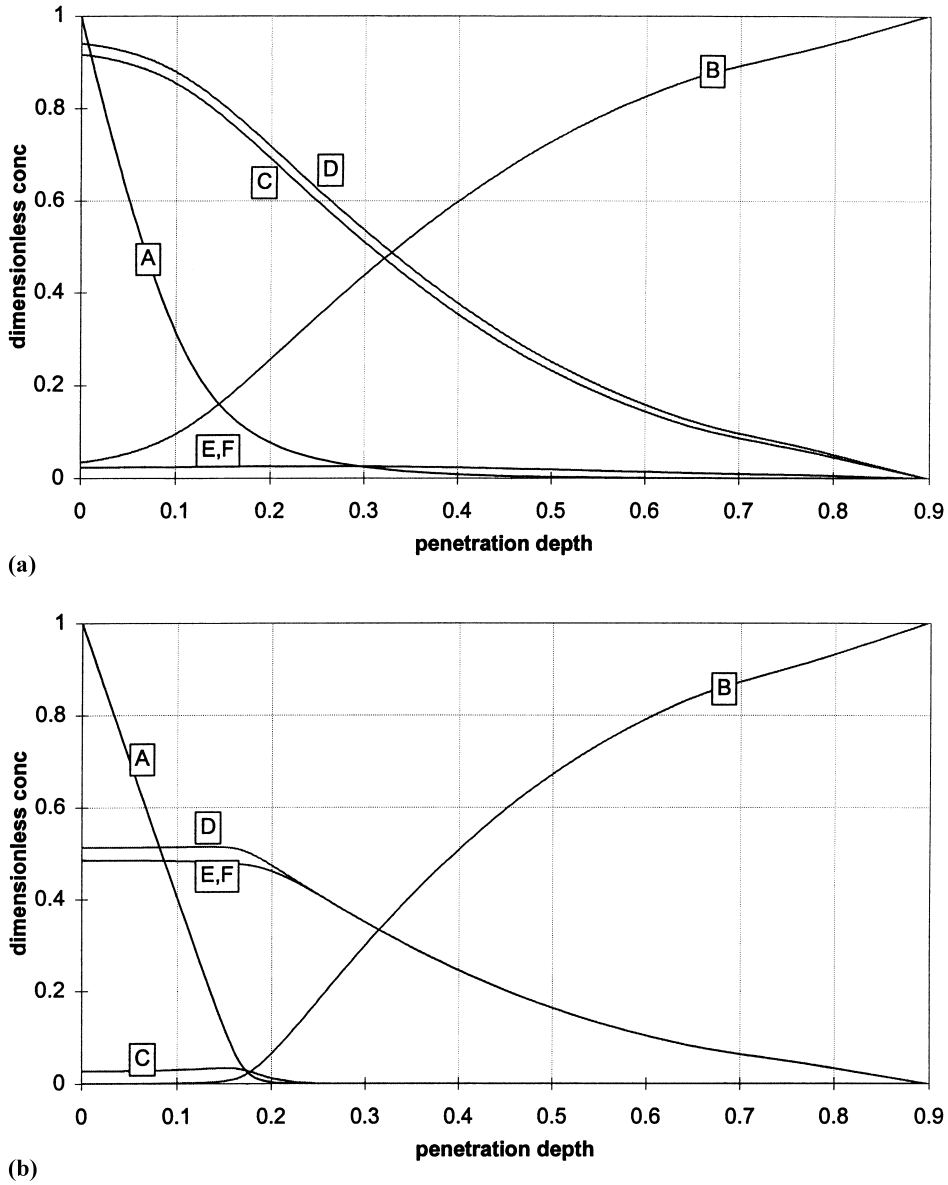

Fig. 4. (a) Case I: Concentration profiles at Ha = 128; $E_A = 4.78$. Reversible-Irreversible Reaction. $K_1 = 100$; $K_{R2} = 10^{-5}$. (b) Case II: Concentration profiles at Ha = 11580; $E_A = 3.09$. Reversible-Irreversible Reaction. $K_1 = 100$; $K_{R2} = 10^{-5}$.

similar to Section 3.2 where the increase in enhancement beyond $E_{\infty 1}$ is caused by the influence of reaction (1c) on the equilibrium of reaction (1b). If, however, the value of $E_{\infty 1}$ is higher than $E_{\infty,\mathrm{irr}}$, then enhancement is reduced proportional to K_2 (Fig. 6c). As explained in Section 3.2, this reduction can be seen as resulting from the competition between A and C for reaction with B, which reduces the absorption of A. This influence of K_2 on the overall enhancement has been predicted earlier [6].

It is interesting to compare the enhancement factor curves for $K_2 = 100$ and two different cases of reaction (1b). In Fig. 2a, (1b) is irreversible ($K_1 \sim \infty$), while in Fig. 6c, $K_1 = 10$. In Fig. 2a, E_A returns to the intermediate enhancement value at very high Hatta numbers (region between Cases III and IV: Fig. 2a). However, when reaction (1b) is reversible, the enhancement drops and remains so till its final infinite value. The occurrence of (1d) which causes the increased enhancement in the instantaneous regime in Fig. 2a does not seem to occur when $K_1 = 10$. Comparing the concentration profiles in the instantaneous regime (Fig. 2e with Fig. 6d), it is clear that in the latter, the reaction plane between A, E and F is not present indicating the absence of (1d). The reversibility of reaction (1b) results in a competitive path for C to react so that the amount reacting to form E and F is less. The lower concentration of E (and F) limits the backward reaction (1c). Thus (1d) cannot occur and the enhancement remains low.

Finally, the model presented in this study was compared to existing analytical solutions for the case where both reac-

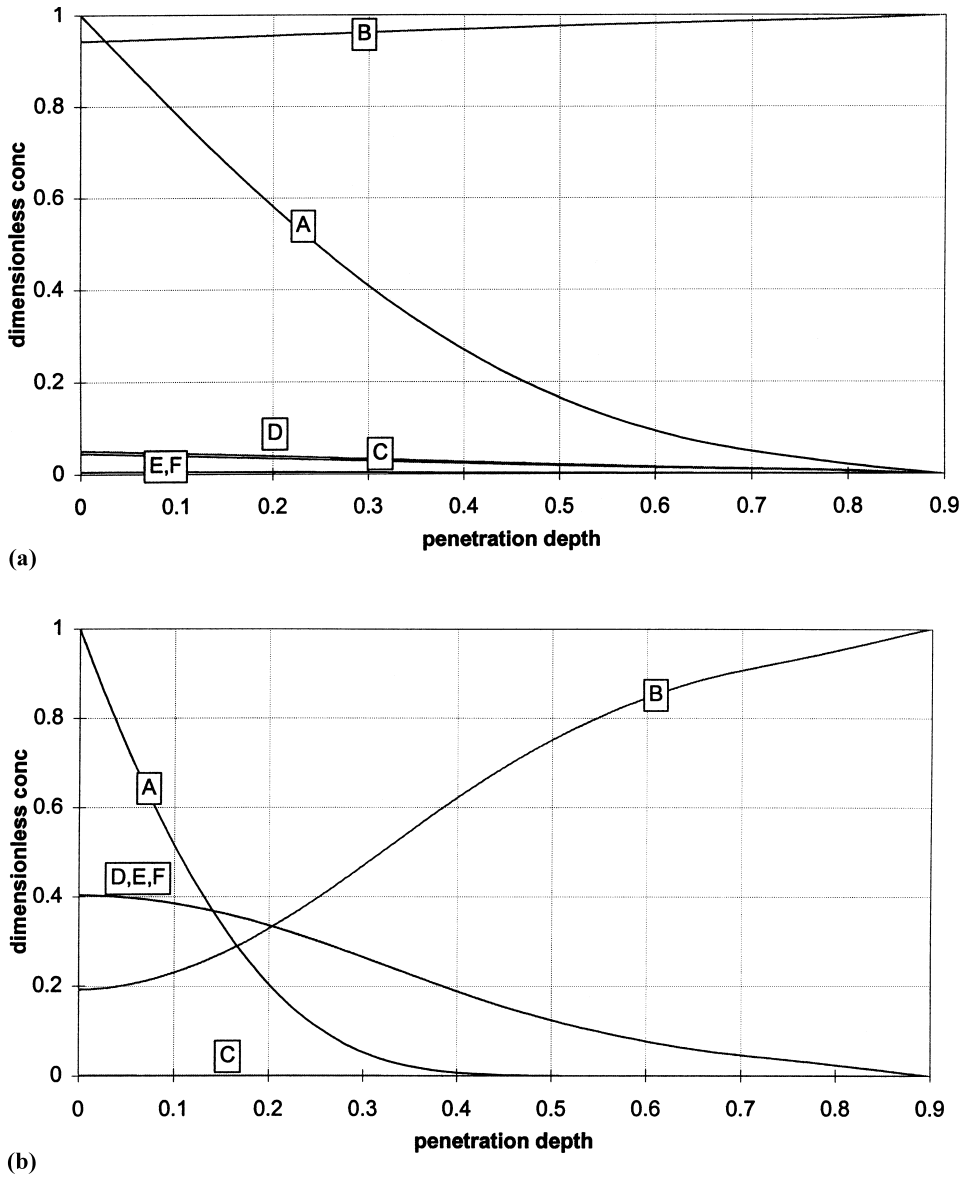

Fig. 5. (a) Case I: Concentration profiles at Ha = 128; $E_A = 1.20$. Reversible-Irreversible Reaction. $K_1 = 0.01$; $K_{R2} = 10^{-5}$. (b) Case II: Concentration profiles at Ha = 11580; $E_A = 2.49$. Reversible-Irreversible Reaction. $K_1 = 0.01$; $K_{R2} = 10^{-5}$.

tions (1b) and (1c) were instantaneous and reversible. The solution presented by Bhattacharya and Ramachandran [6], was used for this purpose (their equation (19)). A maximum deviation of 0.02% was seen for the case of equal diffusivities of all components.

4. Effect of reactant diffusivities

Variation in diffusivity of the reaction species can significantly alter the mass transfer behaviour of multi-step reactions. This has been previously shown for the case of parallel reversible reactions [7]. A similar analysis for two-step reactions is presented below.

4.1. Diffusivity of A

For fixed equilibrium constants ($K_1 = K_2 = 100$), r_A has been varied between two extreme values (Fig. 7a). A change in diffusivity of A alters the value of E_∞ camouflaging secondary effects on enhancement. However, from Fig. 7a, it is clear that, beyond $E_{\infty 1}$, reduction in enhancement is greater for a lower value of r_A. Formation of C in the reaction zone between A and B diffuses towards the bulk where it reacts with B. The lower mobility of A favours reaction (1c) resulting in a greater reduction in enhancement. On further increasing the Hatta number, the system enters the instantaneous reaction regime where additional enhancement is provided by (1d). Lower the mobility of A, greater is the in-

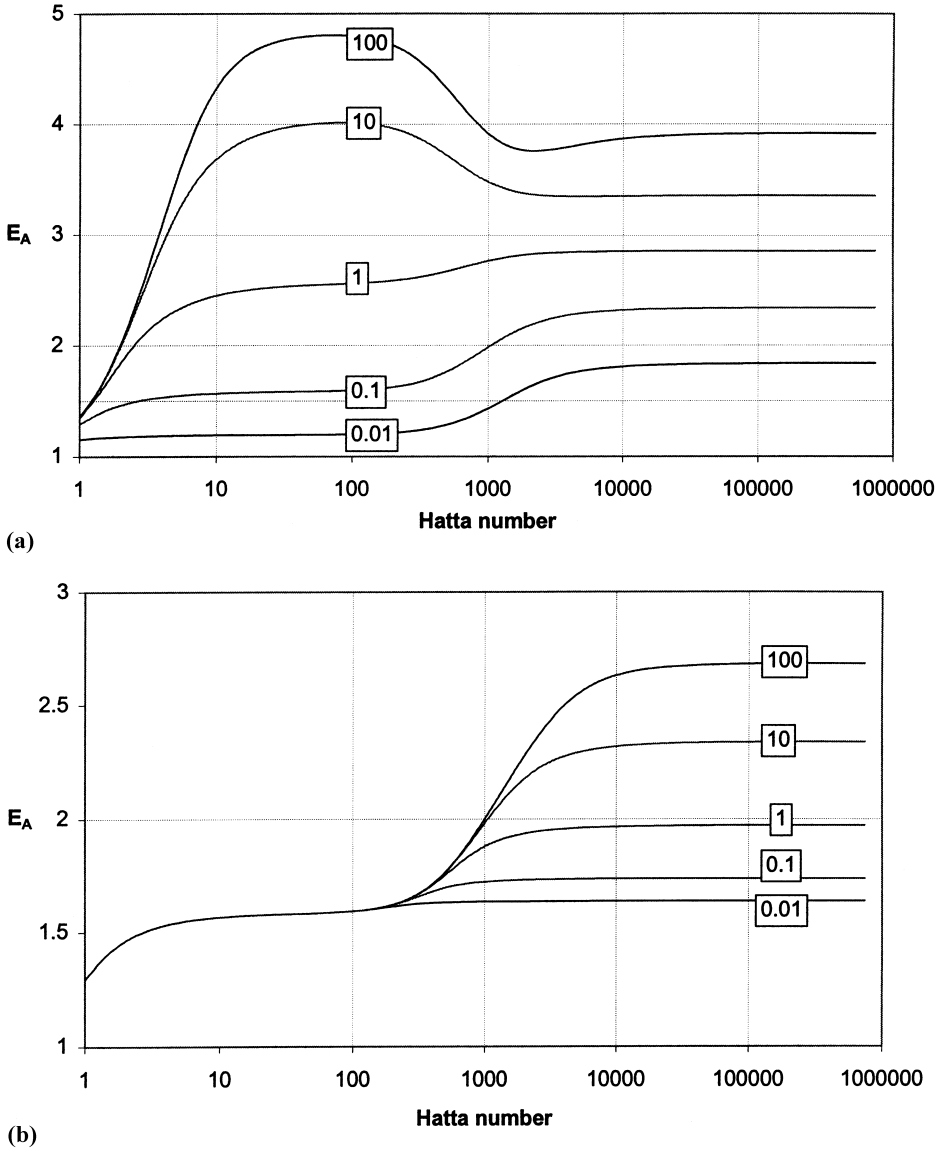

Fig. 6. (a) Effect of K_1 on enhancement factor. Both reactions reversible; $K_2 = 10$ and $K_{R2} = 10^{-5}$. (b) Effect of K_2 on enhancement factor. Both reactions reversible; $K_1 = 0.1$ and $K_{R2} = 10^{-5}$. (c) Effect of K_2 on enhancement factor. Both reactions reversible; $K_1 = 10$ and $K_{R2} = 10^{-5}$. (d) Concentration profiles at Ha $= 7.41 \times 10^5$; $E_A = 3.15$. $K_1 = 10$; $K_2 = 100$; $K_{R2} = 10^{-5}$. $k_L = 9.77 \times 10^{-8}$; $k_{1,1} = 1.30 \times 10^5\ m^3\ mol^{-1}\ s^{-1}$.

crease in enhancement in this regime. The reaction zone of A with E (and F) shifts towards the interface for the case of low r_A, thereby resulting in a higher gradient of A near the interface and, consequently, a higher enhancement. To check this hypothesis, the infinite enhancement was compared for an increased $r_C = 10$.

Fig. 7b shows the effect of K_1 on enhancement for a case where $r_A = 0.1$ and $K_2 = 100$. It is interesting to compare curves for $K_1 = 100$ with the case where both reactions are irreversible (dashed line). The value of $E_{\infty 1}$ for the irreversible case is higher than for $K_1 = 100$ due to the backward reaction of (1b), which, although small, can still cause a slight reduction in enhancement in comparison to the irreversible case. As both reactions become instantaneous with respect to mass transfer (typically for Ha $> 10^6$), enhancement for the irreversible case is lower than that for $K_1 = 100$. When both reactions are irreversible, E_∞ is determined by (8). However, for $K_1 = 100$, infinite enhancement is determined by (1d) which provides additional enhancement. For low mobility of A, this increase can be large enough to make the overall enhancement greater than that for the case when both reactions are irreversible. This increase in enhancement, as explained earlier, is due to the shift in the reaction zone of A with E (and F) towards the interface. Conversely, a smaller difference in enhancements for the irreversible case and $K_1 = 100$ should be observed if r_A is increased. Simulations showed that for $r_A = 0.1$, E_∞ is 8.4 ($E_{\infty,irr} = 6.8$) while for the same K_1 and $r_A = 10$, E_∞ is 2.4 ($E_{\infty,irr} = 2.3$).

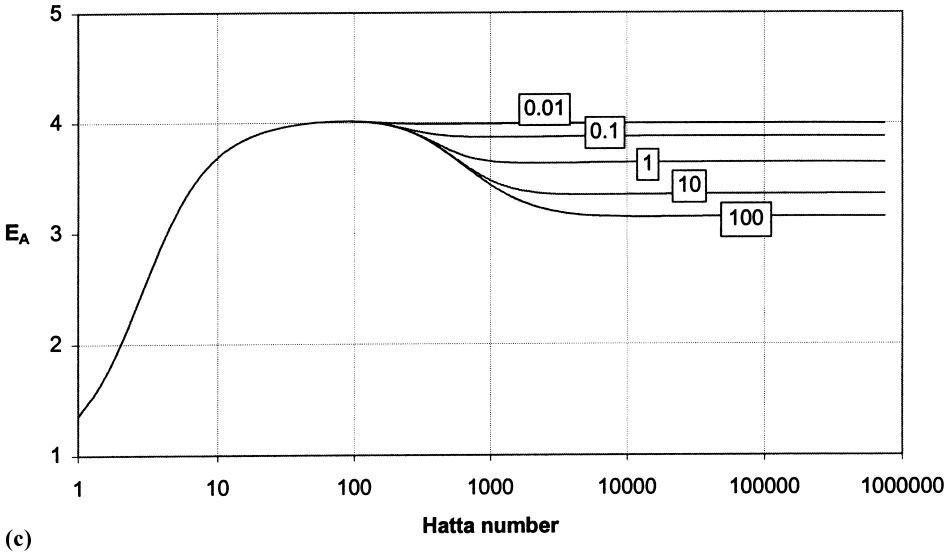

(c)

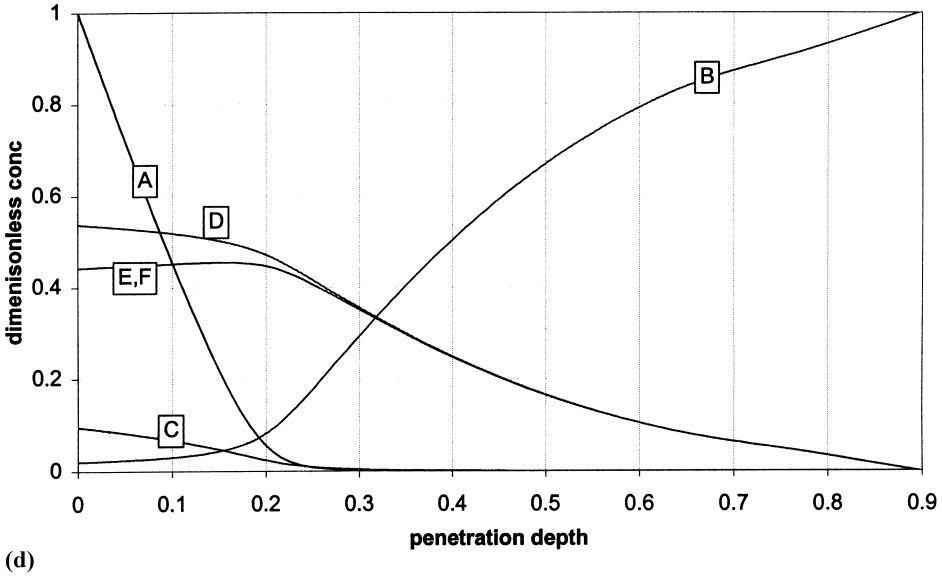

(d)

Fig. 6. (*Continued*).

4.2. Diffusivity of B

Since B reacts via two paths ((1b) and (1c)), the effect of the diffusivity of B on the overall rate of mass transfer was investigated. A change in K_1 affects the characteristics of reaction (1b), which is the same as any single reversible reaction. As a result, simulations presented here have been carried out for a fixed K_1 ($K_1 = 100$) while r_B has been varied between 0.1 and 10.

4.2.1. Effect of r_B on enhancement

The influence of the mobility of B on enhancement is shown in Fig. 8a for a fixed $K_2 = 100$. The value of $E_{\infty 1}$ is higher for a greater mobility of B as is the case for any single reversible reaction. Beyond $E_{\infty 1}$, the drop in enhancement increases as r_B increases as well. C formed by reaction (1b) remains within the penetration depth due to its lower mobility as compared to B. In addition, fresh B easily moves from the bulk into the penetration depth where it consumes the C present (which is closer to the bulk as compared to A) resulting in a greater reduction in the absorption rate of A. The increase in enhancement in the instantaneous reaction regime caused by (1d) is not observed in Fig. 8a since the value of K_3 for this simulation is unity. In addition, r_B does not influence (1d) as B does not directly play a role in the reaction.

4.2.2. Effect of K_2 on enhancement

High mobility of B ($r_B = 10$): From Fig. 8b it is observed that for low values of K_2 ($K_2 = 0.01$), the backward reaction (1c) is large enough to prevent reduction in enhancement beyond $E_{\infty 1}$. In the instantaneous reaction regime, there

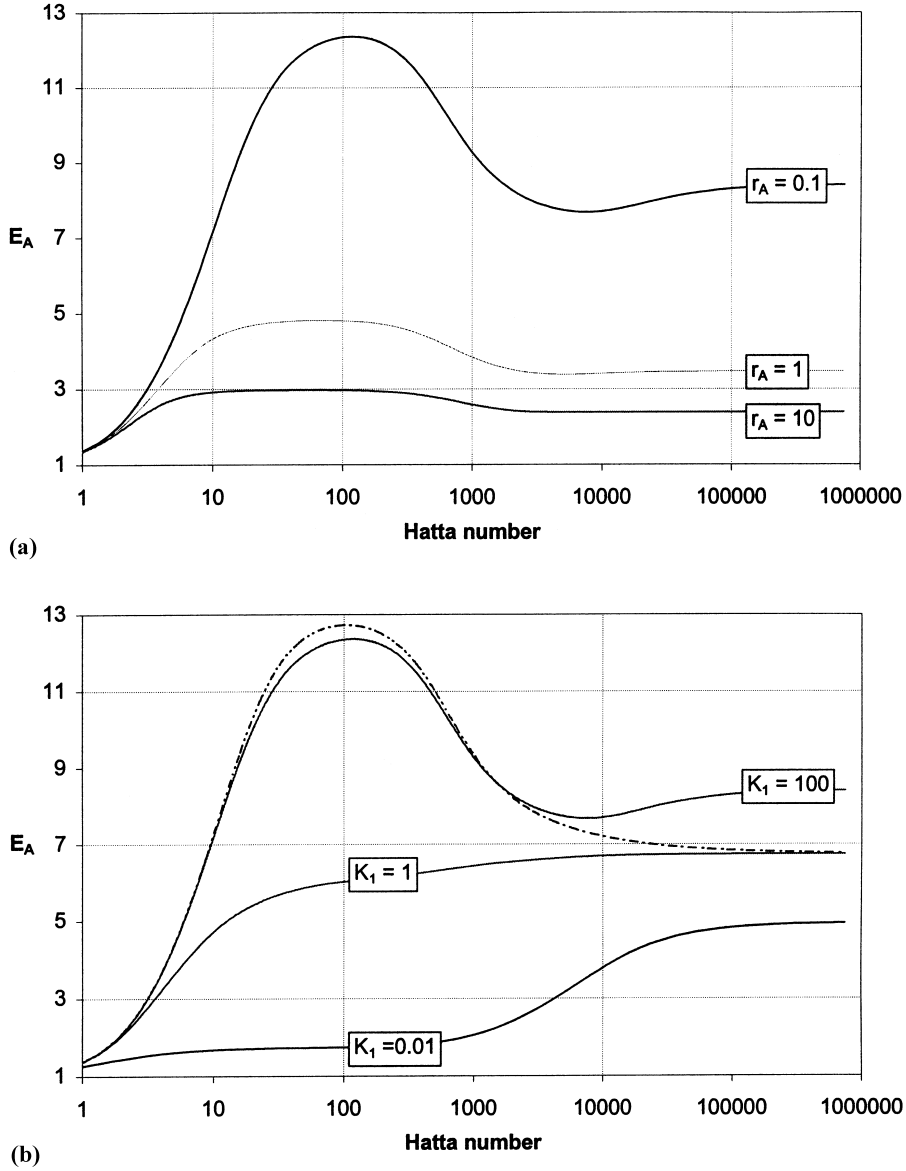

Fig. 7. (a) Effect of r_A on enhancement factor $K_1 = K_2 = 100$ and $K_{R2} = 10^{-5}$. (b) Unequal diffusivity of A-effect of K_1 on enhancement factor. $K_2 = 100$; $K_{R2} = 10^{-5}$ and $r_A = 0.1$. Dashed line indicates the case when both reactions are irreversible.

is no increase in enhancement as would be expected by the effect of (1d). At these high Hatta numbers, sufficient E and F are available for the backward reaction of (1c) to occur. However, the B formed by this reaction (occurring closer to the bulk) moves into the bulk due to its higher mobility instead of moving to the interface where it can react with A. This, in turn, prevents (1d) from occurring.

Low mobility of B ($r_B = 0.1$): As is observed in Fig. 8c, with an increase in the Hatta number beyond $E_{\infty 1}$, the enhancement reduces. As the Hatta number is increased further, sufficient E and F are formed so that the backward reaction (1c) can occur. This regenerates B closer to the interface allowing it to react with A via reaction (1b) and increasing enhancement once again. Thus, even though the mobility of B is low, it is transported towards the interface in the form of more mobile E (and F).

4.3. Diffusivity of C

Simulations were carried out for K_1 and K_2 varying from 0.01 to 100 while r_C was changed between two extreme values of 0.1 and 10 in order to exaggerate its effect so as to understand the underlying phenomena. Simulations for $K_1 = K_2 = 100$ are given in Fig. 9. The main points of interest are given below:

- The value of $E_{\infty 1}$ increases at higher r_C. Greater mobility of C facilitates its movement out of the penetration depth and reduces the rate of the backward reaction (1b). This results in a higher enhancement factor.

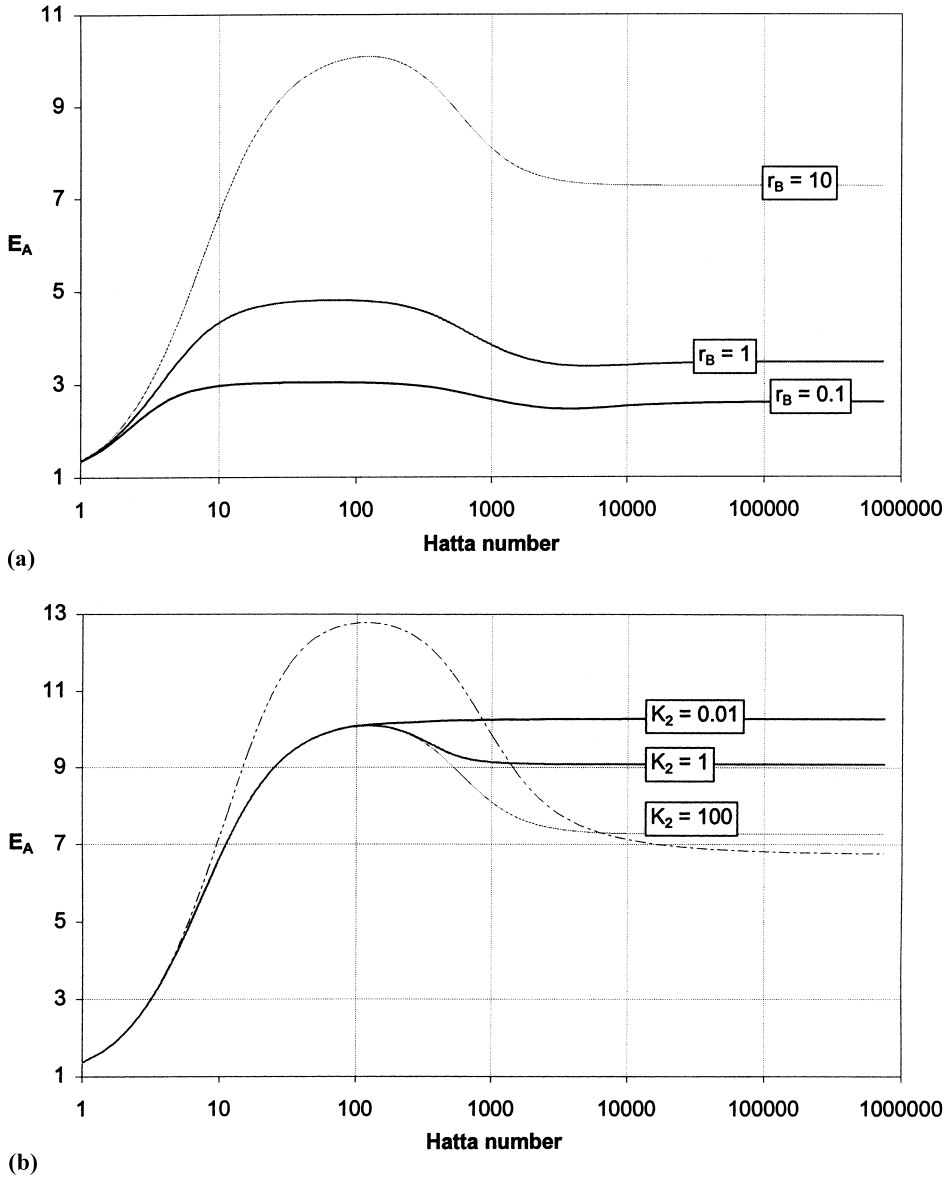

Fig. 8. (a) Effect of r_B on enhancement factor $K_1 = K_2 = 100$ and $K_{R2} = 10^{-5}$. (b) Unequal diffusivity of B-effect of K_2 on enhancement factor. $K_1 = 100$; $K_{R2} = 10^{-5}$ and $r_B = 10$. Dashed line indicates the case when both reactions are irreversible. (c) Unequal diffusivity of B-effect of K_2 on enhancement factor. $K_1 = 100$; $K_{R2} = 10^{-5}$ and $r_B = 0.1$. Dashed line indicates the case when both reactions are irreversible.

- In the instantaneous reaction regime, a higher mobility of C results in it being transported towards the bulk resulting in a shift of the equilibrium towards the side of the products. This, in turn, increases the absorption of A and, consequently, a higher value of E_∞ is obtained for a higher r_C.
- A local minimum in enhancement (E_{min}) is observed in the figure. The value of ΔE_A, defined by (10), increases with increasing r_C. Increased mobility of C reduces the rate of reaction between C and B (via (1c)) so that the drop in enhancement (from $E_{\infty 1}$) is less. However, the increase in enhancement on account of (1d) is greater for higher r_C values due to the stoichiometry of C in the reaction (1d). Hence, a sharper rise in enhancement is observed for higher r_C values. These two opposing factors result in an overall increase in ΔE_A with a rise in r_C.

4.4. Diffusivity of other components

Simulations have shown that the effects of diffusivity of other components (namely D, E and F) give rise to variations in enhancement that can be easily predicted based on mobility of reaction species.

5. Effect of solute loading

In order to study the mass transfer behaviour into loaded solutions, calculations were carried out at varied solute load-

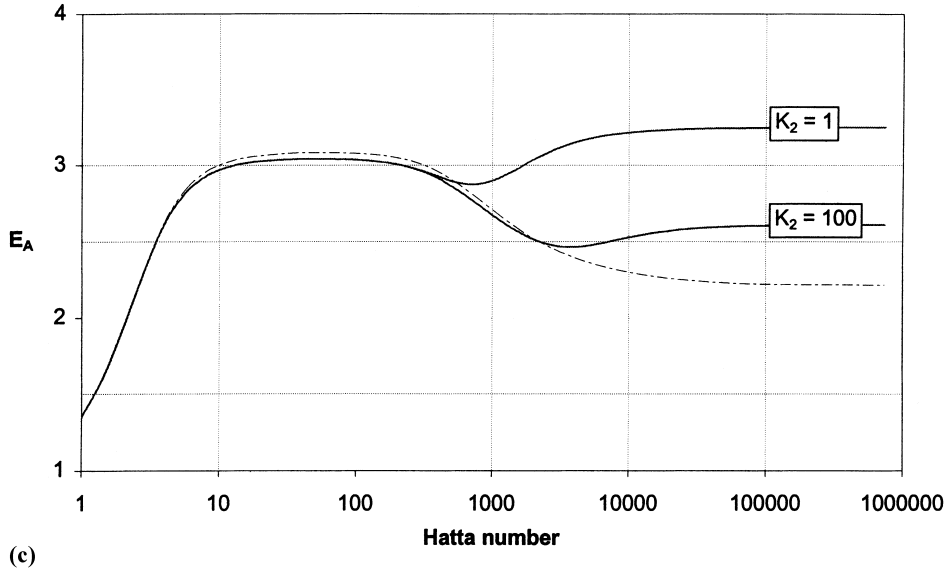

(c)

Fig. 8. (*Continued*).

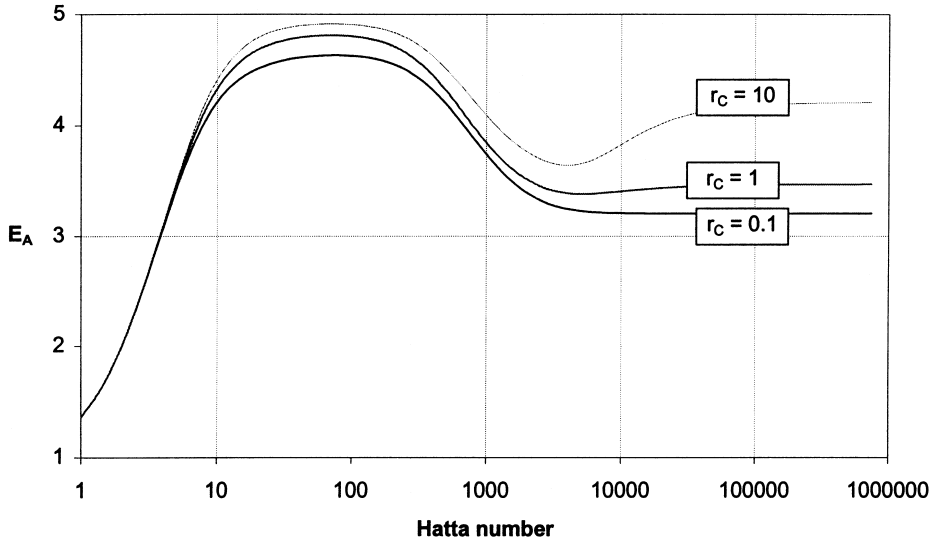

Fig. 9. Effect of r_c on enhancement factor $K_1 = K_2 = 100$ and $K_{R2} = 10^{-5}$.

ing. Bulk equilibrium concentrations were calculated using the equations presented in Section 2.1. The effect of an increase in solute loading on enhancement is presented in Fig. 10 ($K_1 < 1$) and Fig. 1 ($K_1 > 1$). The following points are of interest:

- In general, enhancement is lower for loaded solutions as compared to the unloaded case. This is obviously due to the influence of backward reaction (1b) on the absorption of A.
- A solute loading of 0.672 in Fig. 10, corresponds to identical bulk and interfacial concentrations of solute ($A_i = 10\,\text{mol}\,\text{m}^{-3}$). Consequently, solute desorption prevails for $\alpha > 0.672$.
- The formation of a minimum in enhancement beyond $E_{\infty 1}$ is reduced in the presence of solute loading. This is clearly observed in Fig. 11. Concentration profiles at $E_{\min}$ have been presented in Fig. 12a ($\alpha = 10^{-3}$) and Fig. 12b ($\alpha = 0.5$). The maximum observed in the profile of E (and F) in Fig. 12a indicates the presence of forward reaction (1c), which is responsible for the reduction in enhancement due to competition between A and C for reaction with B. On the other hand, there is no significant formation of E (and F) in Fig. 12b indicating the absence of this competition. Two reasons exist for this — the relatively lower concentration of B in the penetration depth for the case of loaded solu-

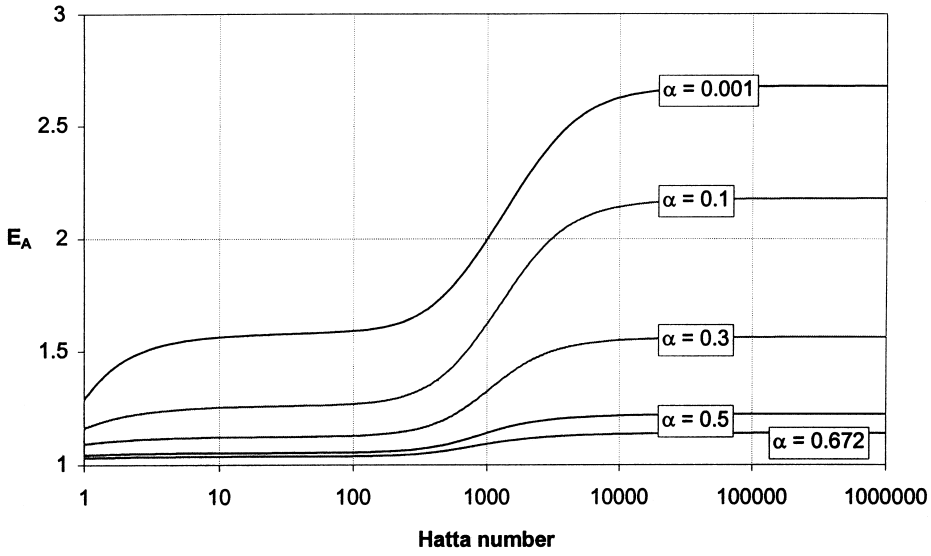

Fig. 10. Effect of solute loading on enhancement factor $K_1 = 0.1$; $K_2 = 100$; $K_{R2} = 10^{-5}$.

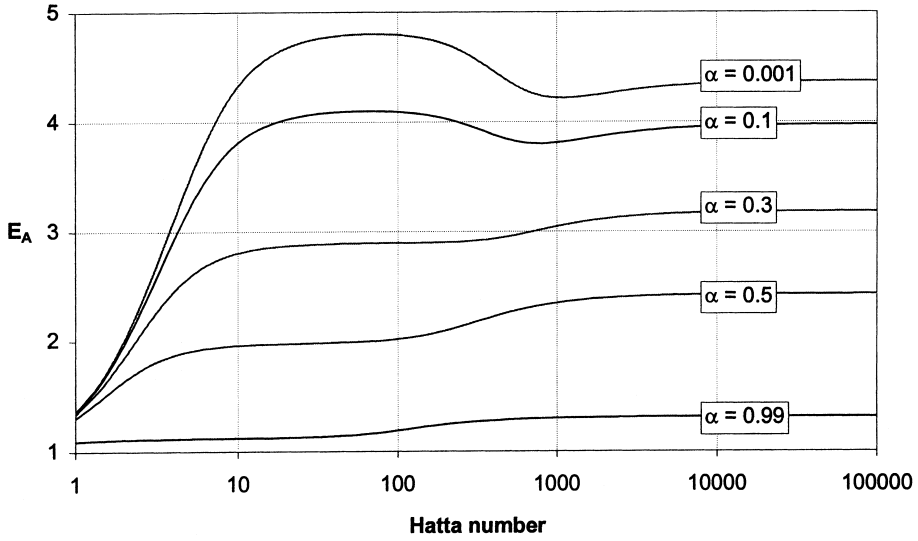

Fig. 11. Effect of solute loading on enhancement factor $K_1 = 100$; $K_2 = 1$; $K_{R2} = 10^{-5}$.

tions and the small rate constant ($K_{R2} = 10^{-5}$) of reaction (1c).

6. Approximate technique to determine E_∞ for reversible two-step reactions

A technique for calculating E_∞ of reversible two-step reactions with equal diffusivities of all chemical species has been derived based on the method described by DeCoursey [8]. This technique is similar to that reported previously for consecutive reactions [4] with corresponding changes in the reaction stoichiometry. The method was used to determine E_∞ for both loaded and unloaded solutions. For unloaded solutions, the initial concentrations of all the chemical species (except B) are taken equal to zero. In case of loaded solutions, for a known set of values of K_1, K_2, α and B_T, the initial concentrations of all other components are obtained by solving Eqs. (5d)–(5g). Results comparing numerical results with those obtained from the approximate solution are presented in Table 5 for loaded solutions ($\alpha = 0.1$). An excellent agreement is observed with a maximum deviation of 0.05%. The maximum deviation for unloaded solutions was 0.02%.

7. Experimental validation of the model developed

7.1. Introduction

The absorption model presented in the previous section has been experimentally validated using the absorp-

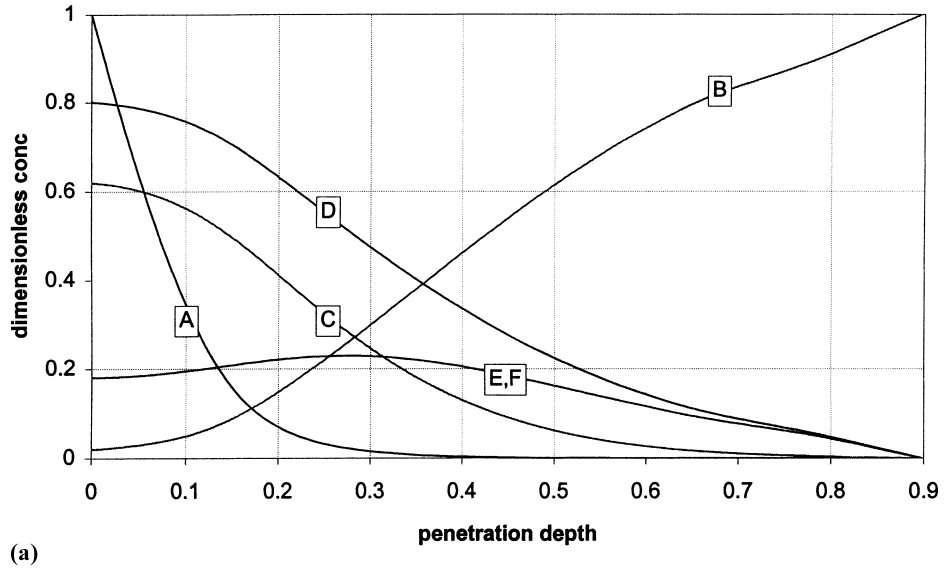

(a)

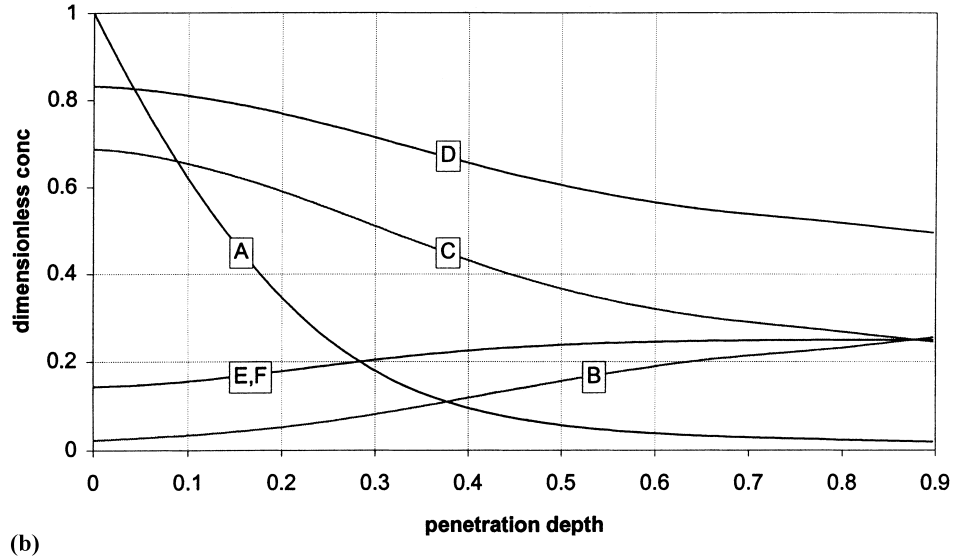

(b)

Fig. 12. (a) Concentration profiles at Ha = 1024; $E_A = 4.22$. $K_1 = 100$, $K_2 = 1$, $K_{R2} = 10^{-5}$ and $\alpha = 10^{-3}$. All components, except A, made dimensionless on initial concentration of B_T (40 mol/m^3). (b) Concentration profiles at Ha = 1024; $E_A = 2.35$. $K_1 = 100$, $K_2 = 1$, $K_{R2} = 10^{-5}$ and $\alpha = 0.5$. All components, except A, made dimensionless on initial concentration of B_T (40 mol/m^3).

tion of CO_2 in NaOH solutions. Further, to study absorption into loaded solutions, the absorption of CO_2 in Na_2CO_3/$NaHCO_3$ mixtures has been chosen. The experimental system is described by the following set of reactions [9]:

$$CO_2 + H_2O \leftrightarrow HCO_3^- + H^+ \quad (11a)$$

$$CO_2 + OH^- \leftrightarrow HCO_3^- \quad (11b)$$

$$HCO_3^- + OH^- \leftrightarrow CO_3^{2-} + H_2O \quad (11c)$$

$$H_3O^+ + OH^- \leftrightarrow 2H_2O \quad (11d)$$

Under alkaline conditions, the contribution of Eq. (11a) to the overall absorption rate is negligible so that the system may be approximated as

$$CO_2 + OH^- \overset{k_{1,1}/k_{1,2}}{\leftrightarrow} HCO_3^- \quad (12a)$$

$$HCO_3^- + OH^- \overset{k_{2,1}/k_{2,2}}{\leftrightarrow} CO_3^{2-} + H_2O \quad (12b)$$

along with the dissociation of water.

$$2H_2O \overset{k_{3,1}/k_{3,2}}{\leftrightarrow} H_3O^+ + OH^- \quad (12c)$$

The corresponding equilibrium constants are defined as

$$K_1 = \frac{HCO_3^-}{CO_2 \cdot OH^-} \quad (13a)$$

$$K_2 = \frac{CO_3^{2-}}{HCO_3^- \cdot OH^-} \quad (13b)$$

Table 5
Comparison of E_∞ obtained numerically with approximate method for loaded solutions ($\alpha = 0.1$)[a]

Numerical		Approximate
$K_2 = 0.01$		
$K_1 = 0.01$	1.17	1.17
$K_1 = 0.1$	1.47	1.47
$K_1 = 1$	2.21	2.21
$K_1 = 10$	3.47	3.47
$K_1 = 100$	4.62	4.62
$K_2 = 0.1$		
$K_1 = 0.01$	1.21	1.21
$K_1 = 0.1$	1.51	1.51
$K_1 = 1$	2.22	2.22
$K_1 = 10$	3.45	3.45
$K_1 = 100$	4.88	4.88
$K_2 = 1$		
$K_1 = 0.01$	1.31	1.31
$K_1 = 0.1$	1.63	1.63
$K_1 = 1$	2.25	2.25
$K_1 = 10$	3.35	3.35
$K_1 = 100$	5.21	5.21
$K_2 = 10$		
$K_1 = 0.01$	1.51	1.51
$K_1 = 0.1$	1.85	1.85
$K_1 = 1$	2.31	2.31
$K_1 = 10$	3.10	3.10
$K_1 = 100$	5.04	5.04
$K_2 = 100$		
$K_1 = 0.01$	1.80	1.80
$K_1 = 0.1$	2.10	2.10
$K_1 = 1$	2.39	2.39
$K_1 = 10$	2.82	2.82
$K_1 = 100$	4.17	4.17

[a]Maximum deviation = 0.05%.

$$K_W = H_3O^+ \cdot OH^- \tag{13c}$$

where K_1 and K_2 are in $m^3\,mol^{-1}$ and K_W in $mol^2\,m^{-6}$.

A list of important previous research on this reaction system is presented in Table 6. All physico-chemical parameters required for the absorption model have been obtained from literature and are given in Appendix A. For the case of loaded solutions, the bulk concentration of each species is determined by simultaneously solving the equilibrium constraints along with a mass balance for the carbon species and an electroneutrality balance.

$$K_1 A_0 B_0 - C_0 = 0, \tag{14a}$$

$$K_2 B_0 C_0 - E_0 = 0, \tag{14b}$$

$$C_{ini} + E_{ini} - A_0 - C_0 - E_0 = 0, \tag{14c}$$

$$H_3O^+ - \frac{K_W}{B_0} = 0, \tag{14d}$$

$$Na^+ + H_3O^+ = B_0 + C_0 + 2E_0, \tag{14e}$$

with $A = CO_2$, $B = OH^-$, $C = HCO_3^-$ and $E = CO_3^{2-}$. C_{ini} and E_{ini} refer to the initial concentrations of Na_2CO_3 and $NaHCO_3$ respectively. These also determine the total Na^+ concentration. The loading factor, as previously described by Eq. (5a), is now modified to,

$$\alpha_{CO_2} = \frac{A_0 + C_0 + E_0}{B_0 + C_0 + 2E_0}. \tag{15}$$

It is important to note that, although the model presented in this study does not account for ionic interactions between the chemical species, no allowance has been made for non-idealities in the experimental validation of the model. All physico-chemical parameters available in literature (such as solubility, diffusivity and rate constants) have been corrected to account for ionic strength. In addition, experiments have been carried out with low ionic strength solutions.

7.2. Approximate solution for enhancement factor

The use of numerical models such as the one presented in this study, can provide precise values of the enhancement factor for multi-step reaction systems. However, their implementation in practice is rather difficult and time consuming, so that simpler solutions — that can be used to determine the value of E_A with sufficient accuracy — are desired. One such approximate solution has been developed by Hikita and Asai [10], for the case when reaction (12a) is irreversible with finite rate and reaction (12b) is reversible and instantaneous. This solution is based on the penetration theory for which the enhancement factor, E_A, is given by

$$E_A = \left(\mathrm{Ha}\cdot\eta + \frac{\pi}{8\mathrm{Ha}\cdot\eta}\right)\mathrm{erf}\left(\frac{2\mathrm{Ha}\cdot\eta}{\sqrt{\pi}}\right) + \frac{1}{2}\exp\left(-\frac{4\mathrm{Ha}^2\cdot\eta^2}{\pi}\right), \tag{16a}$$

where η is given by

$$\eta^4 + \left(\frac{E_A - E_{\infty,\mathrm{irr-irr}}}{E_{\infty,\mathrm{irr-rev}} - 1} + \sqrt{\frac{D_C}{D_B}}\cdot\frac{C_0}{B_0} + \sqrt{\frac{D_C}{D_E}}\cdot\frac{C_0}{E_0}\right)\eta^2 + \left(\frac{E_A - E_{\infty,\mathrm{irr-rev}}}{E_{\infty,\mathrm{irr-rev}} - 1}\right)\left(\sqrt{\frac{D_C}{D_B}}\cdot\frac{C_0}{B_0} + \sqrt{\frac{D_C}{D_E}}\cdot\frac{C_0}{E_0}\right) = 0. \tag{16b}$$

For the CO_2–NaOH system, Hikita et al. [11], assumed that the ratio $(C_0/B_0) = 0$, which is observed when pH > 13. In addition, the value of (C_0/E_0) in (16b) was taken equal to $(K_2B_0)^{-1}$. The value of $E_{\infty,\mathrm{irr-rev}}$, in Eq. (16b) cannot be obtained analytically for all values of K_2. In order to overcome this, Hikita proposed to use the value of $E_{\infty,\mathrm{irr-rev}}$ for the case when $K_2 \to \infty$ (but $K_1/K_2 \to \infty$). Then $E_{\infty,\mathrm{irr-rev}}$ can be obtained by solving Eqs. (17a)–(17c) simultaneously.

$$E_{\infty,\mathrm{irr-rev}} = \frac{1}{\mathrm{erf}\,(\sigma_1)}, \tag{17a}$$

Table 6
Review of previous important research on CO_2 absorption in NaOH and bicarbonate buffer solutions

Authors	Scope	Experimental remarks	Mass transfer analysis
Pinsent and Roughton [20]	Determination of $k_{1,1}$ (T = 0–10°C)	Gas pressure drop analysis. Influence of ionic strength	–
Pinsent et al. [21]	Determination of $k_{1,1}$ (T = 0–40°C)	Thermal method of analysis. Direct reaction of CO_2 with NaOH	–
Himmelblau and Babb [22]	Determination of $k_{1,1}$ and $k_{1,2}$ (T = 0–40°C)	Radioactive tracer analysis. Elimination of mass transfer resistance	–
Danckwerts and Kennedy [23]	Absorption in rotating drum contactor (NaOH and alkaline buffers)	Determination of solubility, diffusivity. Short contact time	Single (1, 2) order instantaneous reaction. Surface renewal theory
Nijsing et al. [24]	Absorption in laminar jet/falling film reactors (up to 2 N solutions)	Short contact time. Low depletion of OH^- at interface	Comparison with asymptotic solutions of pseudo first-order and single (1, 2) order instantaneous reactions
Roberts and Danckwerts [25]	Absorption in wetted wall column (NaOH and alkaline buffers)	Catalytic effect of arsenite ions. Influence of ionic strength on $k_{1,1}$	Comparison with pseudo first-order reaction
Rehm et al. [9]	Absorption in laminar jet reactor (up to 0.1 N NaOH)	Short contact time	Comparison with two-step irreversible reactions. Numerical description for unsteady state absorption
Hikita et al. [11]	Absorption in laminar jet and wetted wall column (NaOH and alkaline buffers)	Absorption in loaded and unloaded solutions	Comparison with two-step reaction with (12b) reversible. Approximate solution based on penetration theory
Pohorecki and Moniuk [16]	Determination of $k_{1,1}$ in laminar jet reactor (up to 4 N NaOH)	Influence of ionic strength with and without co-electrolytes	–

$$2\mathrm{erfc}\left(\sqrt{\frac{D_A}{D_B}}\cdot\sigma_2\right)\exp\left\{\left(\frac{D_A}{D_C}-1\right)\sigma_1^2+\left(\frac{D_A}{D_B}-\frac{D_A}{D_C}\right)\sigma_2^2\right\}=\sqrt{\frac{D_B}{D_A}}\cdot\frac{B_0}{A_i}\mathrm{erf}(\sigma_1), \quad (17b)$$

$$\mathrm{erfc}\left(\sqrt{\frac{D_A}{D_E}}\cdot\sigma_1\right)\exp\left\{\left(\frac{D_A}{D_E}-1\right)\sigma_1^2\right\}-2\mathrm{erfc}\left(\sqrt{\frac{D_A}{D_E}}\cdot\sigma_2\right)\exp\left\{\left(\frac{D_A}{D_C}-1\right)\sigma_1^2+\left(\frac{D_A}{D_E}-\frac{D_A}{D_C}\right)\sigma_2^2\right\}=\sqrt{\frac{D_E}{D_A}}\cdot\frac{E_0}{A_i}\mathrm{erf}\,(\sigma_1)\,. \quad (17c)$$

This value of $E_{\infty,\mathrm{irr-rev}}$ is contrary to the assumption put forward by Hikita and Asai [10] who claim that the approximate solution proposed by them assumes reaction (12b) as instantaneous and reversible.

The value of $E_{\infty,\mathrm{irr-irr}}$ is obtained from Eqs. (18a) and (18b).

$$E_{\infty,\mathrm{irr-irr}}=\frac{1}{\mathrm{erf}\,(\sigma')}, \quad (18a)$$

$$2\mathrm{erfc}\left(\sqrt{\frac{D_A}{D_B}}\cdot\sigma'\right)\exp\left\{\left(\frac{D_A}{D_B}-1\right)\sigma'^2\right\}=\sqrt{\frac{D_B}{D_A}}\cdot\frac{B_0}{A_i}\mathrm{erf}\,(\sigma')\,. \quad (18b)$$

7.3. Experimental validation

Enhancement factors for the absorption of CO_2 in NaOH solutions and $Na_2CO_3/NaHCO_3$ solutions were determined in two different model contactors — namely, a laminar jet reactor (LJR) and a stirred cell reactor (SCR). A brief description of the experimental procedure for each reactor type is given below.

7.3.1. Laminar jet reactor

7.3.1.1. Description of set-up: An LJR was used to study the absorption behaviour of CO_2 in NaOH solutions at short contact times (~0.01–0.03 s) corresponding to low Hatta numbers ($1 < Ha < 10$). The schematic configuration of the experimental set-up is presented in Fig. 13. An NaOH solution of desired strength was prepared in a storage tank (40 l) and maintained under an inert atmosphere. Liquid from the storage vessel was pumped through a thermostat bath by means of a non-pulsating gear pump and finally to the nozzle within the laminar jet reactor where it was ejected in the form of a steady jet. The liquid was collected by a second capillary at the reactor outlet and then fed to a waste tank via a constant level device. Liquid flow rate at the reactor inlet was measured by means of a liquid flow meter while liquid temperature was measured at the reactor inlet and outlet.

CO_2 from a gas cylinder was bubbled through demineralised water to pre-saturate the gas before passing it through a thermal mass flow meter after which it was flown through the reactor. Temperature of the water in the pre-saturator was maintained identical as the temperature of the NaOH solution at the reactor inlet. Further, the gas tubing was lined

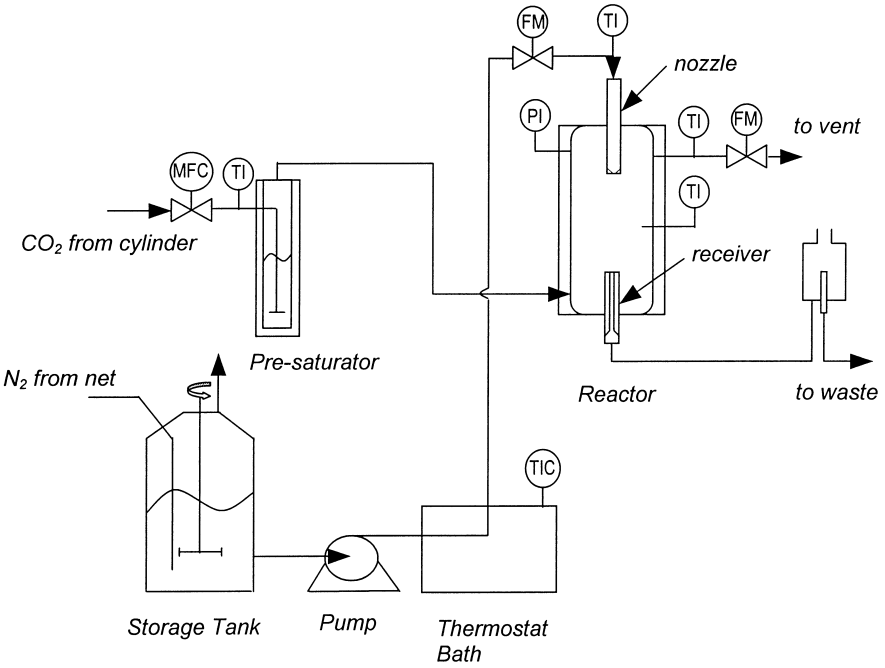

Fig. 13. Experimental set-up of the laminar jet reactor.

with electric heating element to maintain a constant gas temperature throughout the apparatus. The gas temperature was measured at the reactor inlet and outlet while gas flow was measured at the reactor outlet.

7.3.1.2. Experimental procedure: A known volume of demineralised water was degassed using nitrogen after which sodium hydroxide pellets were added under stirring to produce a solution of desired strength. The exact alkali strength was determined by titration against standard acid (0.1 N HCl). The thermostat bath as well as the pre-saturator was set at the desired temperature and CO_2 was allowed to flow through the reactor for sufficient time (usually overnight) to eliminate any inerts. Liquid from the storage tank was then pumped through the reactor and the jet was prepared using the constant level device. The precise jet dimensions were determined by means of a cathetometer (least count = 50 μm.). Once steady state (with respect to liquid flow and temperature) was achieved, the gas flow rate at the reactor outlet was measured. The liquid flow was then stopped and the gas flow rate was allowed to reach its steady state once more. Its value in the absence of liquid flow was then noted. The difference in the gas flow rate, in the presence and absence of liquid flow, was used to determine the gas absorption flux. Experiments were repeated by changing the gas–liquid contact time in two ways — by varying the liquid flow rate or the jet height.

7.3.2. Stirred cell reactor

7.3.2.1. Description of set-up: The stirred cell set-up was used to determine absorption flux of CO_2 in NaOH solutions as well as into aqueous Na_2CO_3/$NaHCO_3$ mixtures. Experiments were carried out in a 95 mm i.d. double-walled glass vessel with a 1.2 l volume. The gas and liquid phase could be stirred separately. The liquid level for all experiments was maintained exactly at halfway the highest blade of the liquid phase stirrer. Stirrer speeds could be varied between 34–51 rpm before disturbances on the liquid surface were visibly observed. Thus, the gas–liquid interfacial area was equal to the geometric area (7.09×10^{-3} m^2). The liquid mass transfer coefficient, k_L, of the reactor was previously determined using the physical absorption of CO_2 in water. Both, the reactor and storage vessel were connected to a thermostat bath to maintain their contents at a desired temperature. In addition, they were also connected to a vacuum line used for degassing. All solutions prepared were stored under vacuum to prevent degradation by atmospheric CO_2. Details of the experimental set-up are presented in Fig. 14.

7.3.2.2. Experimental procedure: A known volume of demineralised water was degassed under vacuum in the storage vessel. Required amounts of chemicals were weighed and added to the water under stirring to obtain solutions of desired strength. The solution was then brought to desired temperature and kept under vacuum. The stirred cell was also evacuated after which the solution from the storage vessel was flown under gravity to a pre-desired level in the cell. The vacuum line was closed and the cell was allowed to reach equilibrium in order to determine the partial pressure of all inerts in the vapour space above the liquid. The cell was then filled with CO_2 till the partial pressure of CO_2 was ca. 1020 mbar. The liquid stirrer was started and the

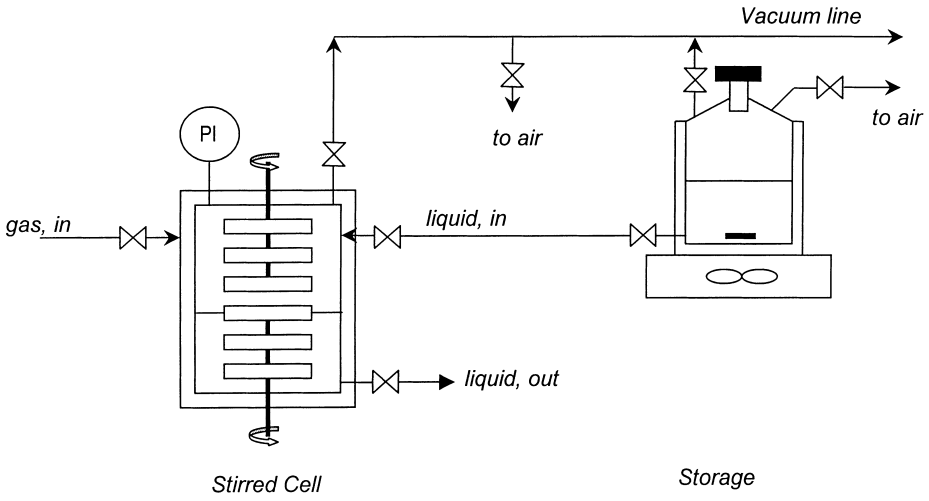

Fig. 14. Experimental set-up of the stirred cell reactor.

pressure drop of CO_2 was measured as a function of time. At the end of the batch time (6 min), the stirrer was stopped and the reactor was opened to air. The reactor contents were drained and the liquid volume determined by weighing.

7.3.2.3. Data analysis: For a batch reactor with gas phase volume, V_G (m^3), a mass balance over the gas phase species, A, yields,

$$V_G \frac{dA_G(t)}{dt} = -E_A k_L a \left(mA_G(t) - A_0\right), \quad (19a)$$

where A_G is the gas phase concentration of CO_2 and a is the gas–liquid interfacial area (m^2).

Integrating Eq. (19a) with initial gas concentration of A of $A_{G,0}$ results in:

$$E_A = \left(\frac{V_G}{k_L a m}\right) \ln\left(\frac{mA_{G,0} - A_0}{mA_G(t) - A_0}\right) \cdot t. \quad (19b)$$

Here it is assumed that the bulk concentration, A_0, does not change within the batch time. This assumption is justified by the fact that the reactions are fast with respect to mass transfer and that in the short batch times the depletion of OH^- is insufficient to allow for accumulation of CO_2 in the liquid bulk. For freshly prepared unloaded solutions, A_0 is nearly equal to zero.

7.4. Results and discussion

7.4.1. Unloaded solutions

Three different NaOH concentrations were used for the absorption of CO_2 as indicated in Table 7. All experiments were carried out at an approximate CO_2 partial pressure of 1020 mbar and $T = 29 \pm 0.1°C$

Fig. 15 compares the experimentally determined enhancement factors (Eq. (19b)) with the values predicted with the flux description presented in the previous chapter for 0.1 M NaOH solution. In addition, the values predicted using the approximate penetration theory solution of Hikita and Asai [10] (see Section 7.2), have also been reported. Deviations using the approximate solution are marginally higher than those obtained with the present model. These deviations can be explained based on the manner in which the parameters for the approximate solution are obtained. Although Hikita and Asai [10] state that reaction (12b) is reversible, the value of $E_{A,irr-rev}$ in their expression (see Eq. (16b)) is calculated by assuming $K_2 \rightarrow \infty$, resulting in Eqs. (17a)–(17c). This inherent irreversibility of reaction (12b) results in a greater competition for the OH^- ion than in reality. Consequently, there is a reduction in the rate of reaction (12a), thereby predicting a lower enhancement than observed.

Deviations between experimental results and the approximate solution increase when the NaOH concentration is reduced to 0.05 M (Fig. 16). For these low values of OH^-, and with the assumption that $K_2 \rightarrow \infty$ results in an increase in the deviation as it exaggerates the competition for the OH^- ion. The numerical model developed in the present study, on the other hand, predicts enhancement factors within the range of experimental error.

A parity plot comparing the experimentally determined enhancement factors and those predicted using the flux description is given in Fig. 17. As observed, an excellent prediction is obtained with the presented model for the entire range of NaOH solutions.

7.4.2. Loaded solutions

In order to check if the present model could successfully account for the variation in ionic strength of the absorbing solution, CO_2 was absorbed into $Na_2CO_3/NaHCO_3$ solutions of varying strengths in an SCR. The systems investigated are presented in Table 8. It is interesting to note that, though the approximate solution gives excellent prediction of the enhancement factor for the system $NaOH/NaHCO_3$, it completely fails for absorption in $Na_2CO_3/NaHCO_3$ solutions. This deviation does not depend on the extent of

Table 7
Systems investigated with model contactors at 29°C

NaOH (N)	Contactor	P_{CO_2} (mbar)	Number of experiments	Average deviation (%) (model)[a]	Average deviation (%) (approximation)[b]
0.250	LJR	970	20	5.6	3.1
0.165	LJR	990	30	5.1	2.8
0.055	LJR	980	60	4.2	4.7
0.250	SCR	1020	32	3.7	3.8
0.100	SCR	1020	33	3.2	4.9
0.050	SCR	1020	39	3.2	8.8

[a]Deviation from model (%) $= \left(\left(E_{A,model} - E_{A,expts.}\right)/E_{A,model}\right)100$.
[b]Deviation from approx. solution (%) $= \left(\left(E_{A,Hikita} - E_{A,expts.}\right)/E_{A,Hikita}\right)100$.

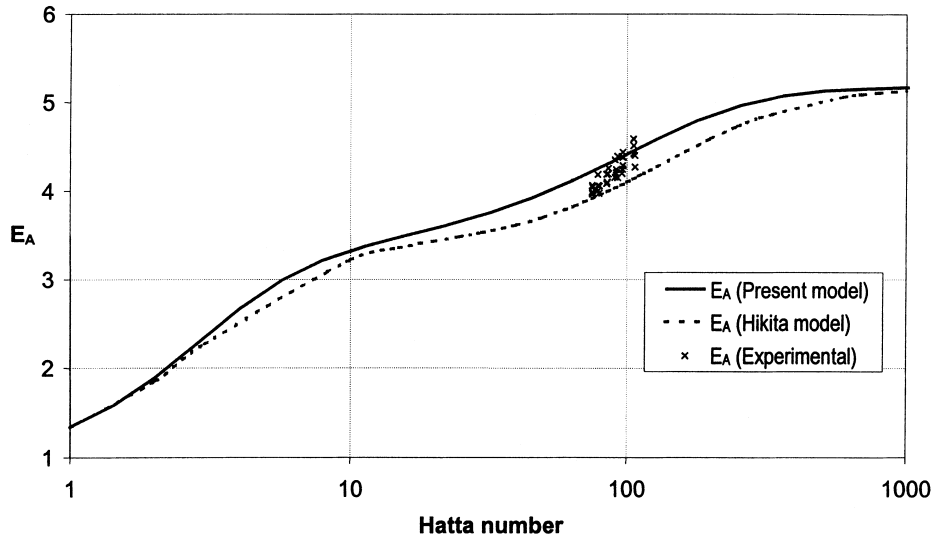

Fig. 15. Comparison of experimentally determined enhancement factors with predicted values. NaOH = 0.1 M; $T = 29°C$; $P_{CO_2} \sim 1020$ mbar.

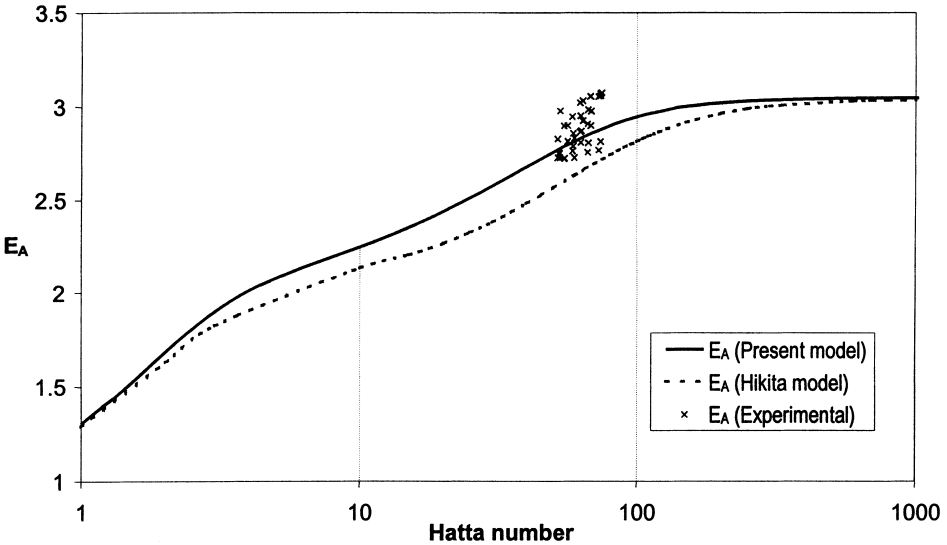

Fig. 16. Comparison of experimentally determined enhancement factors with predicted values. NaOH = 0.05 M; $T = 29°C$; $P_{CO_2} = 1020$ mbar.

solute loading as defined by α_{CO_2} but depends instead on the ratio of carbonate to bicarbonate ions in the liquid bulk (see Table 8). Fig. 18a shows the variation of enhancement factor with Hatta number as obtained using the numerical and approximate solution along with the experimental values for a solution containing $NaHCO_3 = 95\,mol\,m^{-3}$ and $Na_2CO_3 = 175\,mol\,m^{-3}$. In order to explain this large deviation between the experimental values and the approxi-

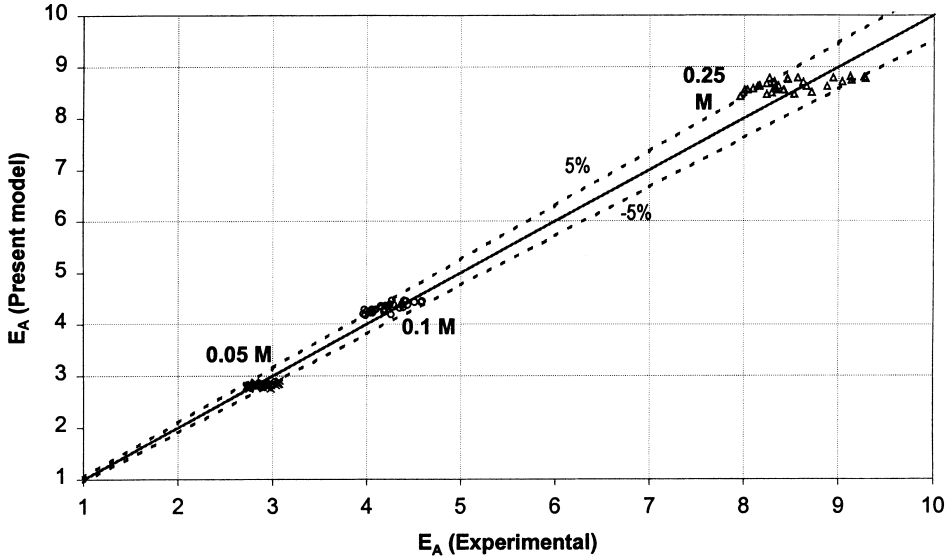

Fig. 17. Parity plot-comparison between experimental and predicted enhancement factors. $T = 29°C$; $P_{CO_2} = 1020$ mbar. Dashed lines indicate percentage deviation.

Table 8
Loaded solutions investigated with SCR at 29°C[a]

NaOH (mol m^{-3})	$NaHCO_3$ (mol m^{-3})	Na_2CO_3 (mol m^{-3})	α_{CO_2}	$HCO_{3,0}^-$ (mol m^{-3})	$CO_{3,0}^{2-}$ (mol m^{-3})	P_{CO_2} (mbar)	Average deviation (%)	
							Model	Approximate
100	250	–	0.71	149.96	99.99	1060	3.1	3.0
–	95	175	0.61	95.16	174.83	1060	5.2	33.0
–	12	100	0.53	12.98	99.02	1020	4.9	23.8

[a]Deviations as defined in Table 7.

mate solution, concentration profiles have been calculated at a fixed Hatta number (see Fig. 18b). The reduction in the concentration of CO_3^{-2} near the interface indicates that at this Hatta number, the backward reaction (12b) takes place which results in the formation of additional OH^- ions and, subsequently, gives rise to additional absorption of CO_2.

The approximate solution underestimates the effect of this backward reaction due to the manner in which the value of $E_{A,irr-rev}$ (used in Eq. (16b)) is obtained. Hikita and Asai [10], have determined this value for the asymptotic case when $K_2 \rightarrow \infty$, where the backward reaction (12b) is neglected. Use of this assumption would not account for the additional enhancement provided by reaction (12b) at these Hatta numbers and, hence, would explain the lower values obtained by the approximate solution as compared to those seen from experiments. It is obvious that this underestimation of the enhancement factor by use of the approximate solution will be greater at higher bulk concentrations of the carbonate ion.

Thus, from the experimental study on CO_2 absorption in caustic and bicarbonate buffers, it has been shown that the model presented in this study successfully predicts the enhancement factor over a wide range of gas–liquid contact times. In addition, it has been shown that the approximate solution as proposed in [10] can predict enhancement factors for unloaded solutions but underestimates the enhancement factor for the case of $NaOH/Na_2CO_3$ solutions.

8. Conclusions

A numerical model based on the Higbie penetration theory for isothermal reversible two-step chemical reactions has been presented in this study.

For irreversible reactions, the results presented in this paper are similar to those obtained by Brian and Beaverstock [2]. For instantaneous reversible reactions, the model was compared with the analytical solution reported in [6]. Maximum deviation of 0.02% was observed.

It has been shown that the shape of the enhancement curves is dependent on the values of the two equilibrium constants. In general, beyond $E_{\infty 1}$, there is a reduction in enhancement caused by the removal of reactant B by reaction (1c). In case of reversible reactions, however, two effects are possible. For a high value of K_1, the approach to E_∞ is from above as the amount of C formed is sufficient to reduce the concentration of B sufficiently to reduce enhancement. However, for low K_1, the approach to E_∞ is from below as C formed does not reduce concentration of B sufficiently, but its removal by reaction (1c) shifts the equilibrium of re-

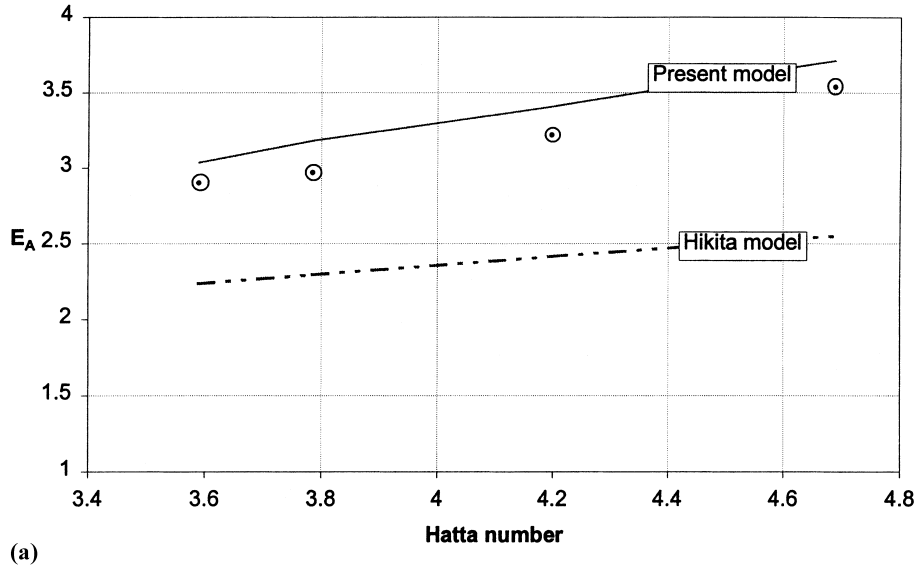

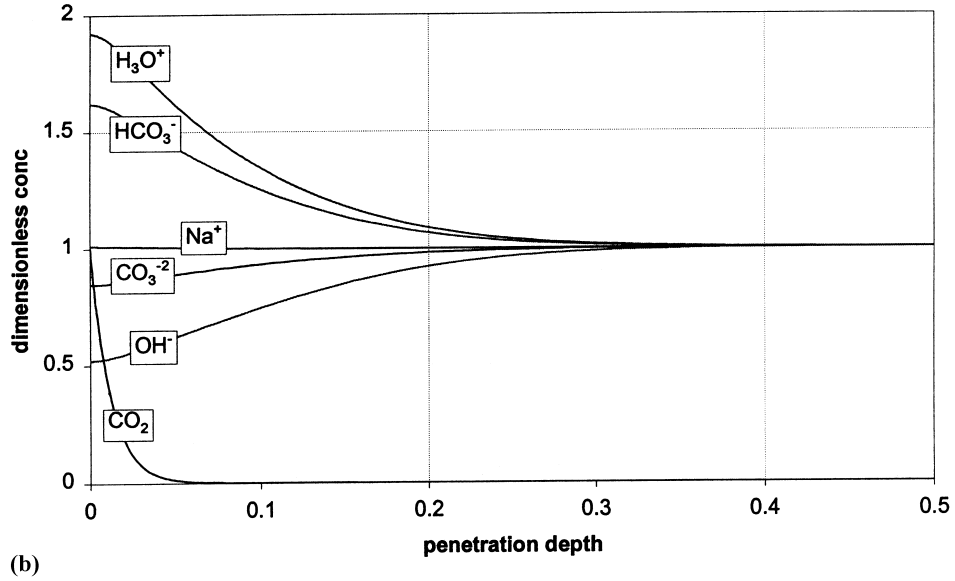

Fig. 18. (a) Comparison of enhancement factors obtained experimetally with prediction from model and approximate solution. $NaHCO_3 = 95\,mol\,m^{-3}$ and $Na_2CO_3 = 175\,mol\,m^{-3}$. Contractor = SCR; P_{CO_2}=1060 mbar; $T = 29^{\circ}C$. ⊙ = Experimental values. (b) Concentration profiles at end of the contact time for system described in Figure 18a. $OH^-_{,0}$=0.188 mol m^{-3}; $HCO^-_{3,0}$=95.16 mol m^{-3}, $CO^{-2}_{3,0}$=174.83 mol m^{-3} $CO_{2,0} = 1.49 \times 10^{-2}$ mol m^{-3}. All concentrations made dimensionless on bulk values except CO_2, which is based on its interfacial value.

action (1b) to the side of the products so that enhancement increases beyond $E_{\infty 1}$. In addition, for instantaneous reaction regime, additional enhancement is provided by reaction (1d). This is a combination of backward reaction (1c) with forward reaction (1b) and its occurrence has been reported earlier [12]. This phenomenon can only be observed in case of reversible reactions.

For the case of unequal diffusivity of the gas component, A, it has been shown that the enhancement, especially in the instantaneous regime, can be higher than the case of irreversible reactions. This is on account of the large additional enhancement caused by reaction (1d) for lower mobility of A. The reaction plane between A and E (and F) shifts towards the interface for low r_A. A similar effect is seen with higher mobility of the intermediate, C.

Enhancement for absorption into loaded solutions is lower than corresponding values for unloaded solutions. The formation of a minimum in enhancement in reduced in the case of loaded solutions due to the limited extent of forward reaction (1c).

An approximate method for determining E_∞ for reversible two-step reactions with equal diffusivities has been developed. This method is based on one presented earlier [8]. The method was checked against numerical results for loaded

and unloaded solutions. A maximum deviation of 0.02% for unloaded solutions was found while the same for loaded solutions ($\alpha = 0.1$) was found to be 0.05%.

The model presented in this study has been validated against experimental values of the enhancement factor for the absorption of CO_2 in NaOH and bicarbonate solutions. Excellent agreement has been observed between the present model and experimental values for a wide range of gas–liquid contact times. It has been shown that the approximate solution of Hikita and Asai [10], underestimates the value of the enhancement factor for loaded solutions. This is attributed to the assumption of irreversibility of reaction (12b) in determining the parameters of the approximate solution.

Nomenclature

A	concentration of component A and CO_2 ($mol\,m^{-3}$)
a	gas–liquid interfacial area (m^2)
B	concentration of component B and OH^- ($mol\,m^{-3}$)
C	concentration of component C and HCO_3^- ($mol\,m^{-3}$)
D	concentration of component D ($mol\,m^{-3}$)
D_{sub}	diffusivity, sub: component ($m^2\,s^{-1}$)
E	concentration of component E and CO_3^{2-} ($mol\,m^{-3}$)
E_∞	final enhancement factor (−)
$E_{\infty 1}$	intermediate asymptotic enhancement factor (−)
$E_{\infty,irr-irr}$	infinite enhancement factor; both (12a) and (12b) irreversible (−)
$E_{\infty,irr-rev}$	infinite enhancement factor; (12a) irreversible and (12b) reversible (−)
E_A	enhancement factor, defined by Eq. (6a) (−)
F	component F, concentration of component F ($mol\,m^{-3}$)
F	Faraday constant = 96 500 ($C\,mol^{-1}$)
Ha	Hatta number, defined by Eq. (6b) (−)
K_1	equilibrium constant of (1b) and Eq. (13a) (−)
K_2	equilibrium constant of (1c) and Eq. (13b) (−)
K_3	equilibrium constant of (1d) (−)
k_G	gas side mass transfer coefficient ($m\,s^{-1}$)
k_L	liquid side mass transfer coefficient ($m\,s^{-1}$)
K_{R2}	ratio of forward rate constants, defined by Eq. (6c) (−)
$k_{sub,1}$	reaction rate constant, sub: reaction number, forward ($m^3\,mol^{-1}\,s^{-1}$)
$k_{sub,2}$	reaction rate constant, sub: reaction number, backward ($m^3\,mol^{-1}\,s^{-1}$)
K_W	ionic product of water ($mol^2\,m^{-6}$)
LJR	laminar jet reactor (−)
m	gas partition coefficient ($A_i/A_{i,G}$) (−)
N_A	absorption flux with reaction ($mol\,m^{-2}\,s^{-1}$)
P	pressure (bar)
R_{A1}	rate of reaction (1b), defined by Eq. (3a) ($mol\,m^{-3}\,s^{-1}$)
R_{A2}	rate of reaction (1c), defined by Eq. (3b) ($mol\,m^{-3}\,s^{-1}$)
r_B	reduced diffusivity of B, defined as $D_B/10^{-9}$ (−)
r_{sub}	reduced diffusivity, defined by D_{sub}/D_B, sub: component (−)
SCR	stirred cell reactor (−)
t	time variable (s)
V	volume (m^3)
x	position variable, (m)
z	ionic charge (−)

Greek

l_i^∞	ionic conductivity at infinite dilution ($m^2\,\Omega^{-1}\,mol^{-1}$)
Δ	additional enhancement caused by (1d), defined by Eq. (10) (−)
η	constant, defined by Eq. (16a) (−)
α	loading factor, defined by Eqs. (5a) and (15) (−)
ρ	density ($kg\,m^{-3}$)
σ'	constant, defined by Eq. (18a) (−)
σ_1	constant, defined by Eq. (17a) (−)
σ_2	constant, defined by Eqs. (17b) and (17c) (−)

Subscripts

∞	infinite dilution
0	bulk condition
g, G	gas phase
I	condition at liquid side of interface; ion type
I, G	gas side interface
ini	initial
irr	irreversible
l, L	liquid phase
min	minimum in enhancement
red	reduced
rev	reversible
T	total
w	water

Superscripts

m, n, p, q	kinetic orders (−)
r, s, u, v	kinetic orders (−)

Appendix A. Physico-chemical parameters

A.1. Physical parameters

A.1.1. Solubility

The solubility of CO_2 in aqueous electrolytic solutions has been estimated using the method presented by Schumpe [13]. The gas distribution coefficient, m, is determined by

Table A.1
Ionic conductivity at infinite dilution [15]

Ion	Ionic conductivity ℓ_i^∞ ($m^2\,\Omega^{-1}\,mol^{-1}$)	Temperature range (K)
Na^+	$(-1.2464 + 0.2312\ln(T))^2$	273.15–373.15
OH^-	$-0.1925 + 1.2291\sqrt{T}$	273.15–373.15
H^+	$0.1724 - 40.8903/T$	273.15–373.15
HCO_3^-	4.45×10^{-3}	298.15
CO_3^{2-}	$3.11 \times 10^{-5} + 2.63 \times 10^{-10}(T)^3$	273.15–298.15

$$\log\left(\frac{m_W}{m}\right) = \left(1.171 \times 10^{-4} - 1.83 \times 10^{-5}\right) Na^+ + \left(7.56 \times 10^{-5} - 1.83 \times 10^{-5}\right) OH^- + \left(1.372 \times 10^{-4} - 1.83 \times 10^{-5}\right) HCO_3^- + \left(1.666 \times 10^{-4} - 1.83 \times 10^{-5}\right) CO_3^{2-}, \quad \text{(A.1a)}$$

where the ionic concentrations are in mol m^{-3}. This expression is valid at 298 K but can be used without loss of accuracy in a temperature range, 293–303 K [13]. The distribution coefficient of CO_2 in pure water, m_w, is taken from [14].

$$m_W = 3.59 \times 10^{-7} \cdot RT \exp\left(\frac{2044}{T}\right), \quad \text{(A.1b)}$$

where R is the universal gas constant (mol m^{-3} K^{-1}) and T is in Kelvin.

A.1.2. Diffusivity

Diffusion coefficient of CO_2 in electrolytes, D_{CO_2}, has been obtained from [11]:

$$\frac{D_{CO_2}}{D_{CO_2,w}} = 1 - \left(1.29 \times 10^{-4} NaOH + 1.4 \times 10^{-4} NaHCO_3 + 2.61 \times 10^{-4} Na_2CO_3\right). \quad \text{(A.2a)}$$

The diffusivity of CO_2 in pure water, $D_{CO_2,w}$ ($m^2\,s^{-1}$) is taken from [14].

$$D_{CO_2,w} = 2.35 \times 10^{-6} \exp\left(\frac{-2119}{T}\right). \quad \text{(A.2b)}$$

Ionic diffusion coefficients at infinite dilution have been estimated using the Nernst equation [15].

$$D_i^\infty = \ell_i^\infty \frac{RT}{z_i F^2}, \quad \text{(A.2c)}$$

where F is the Faraday constant.

The ionic conductivity at infinite dilution of the various ions, ℓ_i^∞, has been fitted as a function of temperature using data available in [15]. These functions have been presented in Table 9.

Appendix B. Chemical parameters

B.1. Kinetic rate constants

An expression for the forward rate constant, $k_{1,1}$, as a function of ionic strength was presented by Pohorechi et al. [16]. The expression given by Eqs. (A.3a) and (A.3b) is valid for absorption into pure NaOH solutions varying from 0.1 to 4 N and for the temperature range, 294–314 K.

$$\log\frac{k_{1,1}}{k_{1,1}^\infty} = 2.21 \times 10^{-4} I - 1.6 \times 10^{-8} I^2, \quad \text{(A.3a)}$$

where the reaction rate constant at infinite dilution, $k_{1,1}^\infty$ is given by:

$$\log k_{1,1}^\infty = 8.895 - \frac{2382}{T} \quad \text{(A.3b)}$$

and the ionic strength, I, is defined as

$$I = \tfrac{1}{2}\left(Na^+ z_{Na^+}^2 + OH^- z_{OH^-}^2\right). \quad \text{(A.3c)}$$

The ionic concentrations are in mol m^{-3} and the corresponding units of $k_{1,1}$ and $k_{1,1}^\infty$ are $m^3\,mol^{-1}\,s^{-1}$.The value of $k_{1,1}$ is modified by the presence of co-electrolytes and is reported by Pohorechi et al. [16] as,

$$\log\frac{k_{1,1}}{k_{1,1}^\infty} = 1.2 \times 10^{-4}\left(\tfrac{1}{2}Na^+ z_{Na^+}^2\right) + 2.2 \times 10^{-4}\left(\tfrac{1}{2}OH^- z_{OH^-}^2\right) + 8.5 \times 10^{-5}\left(\tfrac{1}{2}CO_3^{2-} z_{CO_3^{2-}}^2\right), \quad \text{(A.4a)}$$

with,

$$\log k_{1,1}^\infty = 11.916 - \frac{2382}{T} \quad \text{(A.4b)}$$

Eqs. (A.4a) and (A.4b) were used for the simulations with loaded solutions. Since the contribution of HCO_3^- to the value of $k_{1,1}$ has not been reported, its influence on the forward rate constant was neglected.

Since reaction (12b) involves proton transfer, it is very rapid. Eigen [17] determined the rates of reactions involving proton or hydroxyl ions in aqueous solutions to be in the order of 10^7 to 10^8 $m^3\,mol^{-1}\,s^{-1}$. Therefore, in the present study, the value of $k_{2,1}$ has been assumed to be

Table B.1
Physico-chemical parameters used in the flux description[a]

Parameter	Units	0.250 N	0.165 N	0.100 N	0.055 N	0.050 N
m	(–)	7.15×10^{-1}	7.37×10^{-1}	7.54×10^{-1}	7.66×10^{-1}	7.68×10^{-1}
$k_{1,1}$	$m^3\,mol^{-1}\,s^{-1}$	1.16×10^{1}	1.12×10^{1}	1.08×10^{1}	1.06×10^{1}	1.05×10^{1}
$k_{1,2}$	s^{-1}	3.41×10^{-4}	3.27×10^{-4}	3.17×10^{-4}	3.09×10^{-4}	3.09×10^{-4}
$k_{2,1}$	$m^3\,mol^{-1}\,s^{-1}$	10^7	10^7	10^7	10^7	10^7
$k_{2,2}$	s^{-1}	1.23×10^{6}	1.38×10^{6}	1.55×10^{6}	1.74×10^{6}	1.77×10^{6}
D_{CO_2}	$m^2\,s^{-1}$	2.05×10^{-9}	2.07×10^{-9}	2.09×10^{-9}	2.10×10^{-9}	2.10×10^{-9}
D_{OH^-}	$m^2\,s^{-1}$	5.72×10^{-9}	5.72×10^{-9}	5.72×10^{-9}	5.72×10^{-9}	5.72×10^{-9}
$D_{HCO_3^-}$	$m^2\,s^{-1}$	1.20×10^{-9}	1.20×10^{-9}	1.20×10^{-9}	1.20×10^{-9}	1.20×10^{-9}
$D_{CO_3^{2-}}$	$m^2\,s^{-1}$	9.83×10^{-10}	9.83×10^{-10}	9.83×10^{-10}	9.83×10^{-10}	9.83×10^{-10}

[a] $T = 29^\circ C$.

$10^7\,m^3\,mol^{-1}\,s^{-1}$. The neutralisation rate constant, $k_{3,2}$, has also been reported as $1.5 \times 10^8\,m^3\,mol^{-1}\,s^{-1}$ [17]. However, the temperature at which this rate constant has been determined is not mentioned.

B.1.1. Equilibrium constants

The value of K_1 may be determined by a combination of Eqs. (11a) and (11d). Edwards et al. [18] have reported the equilibrium constant of Eq. (11a) as

$$K_3 = \frac{H^+ \cdot HCO_3^-}{CO_2} = \exp\left(\frac{-12092.1}{T} - 36.786\ln(T) + 235.482\right)\rho_W, \quad (A.5a)$$

where ρ_w is the density of water ($kg\,m^{-3}$).

The solubility product, K_w ($mol^2\,m^{-6}$), has been taken from [19].

$$K_W = H^+ \cdot OH^- = 10^{5839.5/T + 22.4773\log T - 61.2062} \cdot \rho_W^2. \quad (A.5b)$$

Both Eqs. (A.5a) and (A.5b) are valid over a temperature range 273–498 K. K_1 ($m^3\,mol^{-1}$) can then be determined as:

$$K_1 = \frac{K_3}{K_W}. \quad (A.5c)$$

Equilibrium constant for reaction (12b), K_2 ($m^3\,mol^{-1}$), has been reported in [11] as a function of ionic strength.

$$\log\left(\frac{K_2}{K_2^\infty}\right) = \frac{3.194 \times 10^{-2}\sqrt{Na^+}}{1 + 4.016 \times 10^{-2}\sqrt{Na^+}} + 1.25 \times 10^{-4} Na^+, \quad (A.6a)$$

with the value at infinite dilution, K_2^∞ given as

$$\log\left(K_2^\infty\right) = \left(\frac{1568.924}{T} + 2.5865 - 6.737 \cdot 10^{-3} T\right). \quad (A.6b)$$

No temperature limitation for K_2 has been reported.

A list of the physico-chemical parameters for the different systems studied is presented in Table 10.

References

[1] W.P.M. van Swaaij, G.F. Versteeg, Chem. Eng. Sci. 47 (1992) 3181–3195.
[2] P.L.T. Brian, M.C. Beaverstock, Chem. Eng. Sci. 20 (1965) 47–56.
[3] G.F. Versteeg, J.A.M. Kuipers, F.P.H. van Beckum, W.P.M. van Swaaij, Chem. Eng. Sci. 44 (1989) 2295–2310.
[4] R.D. Vas Bhat, J.A.M. Kuipers, G.F. Versteeg, Chem. Eng. Sci. 54 (1999) 121–136.
[5] P.A. Ramachandran, Chem. Eng. Sci. 27 (1972) 1807–1816.
[6] A. Bhattacharya, P.A. Ramachandran, Chem. Eng. J. 25 (1982) 115–218.
[7] G.F. Versteeg, J.A.M. Kuipers, F.P.H. van Beckum, W.P.M. van Swaaij, Chem. Eng. Sci. 45 (1990) 183–197.
[8] W.J. DeCoursey, Chem. Eng. Sci. 37 (1982) 1483–1489.
[9] T.R. Rehm, A.J. Moll, A.L. Babb, AIChE J. 9 (1963) 760–765.
[10] H. Hikita, S. Asai, J. Chem. Eng. 11 (1976) 123–129.
[11] H. Hikita, S. Asai, T. Takatsuka, Chem. Eng. J. 11 (1976) 131–141.
[12] H. Hikita, S. Asai, T. Takatsuka, Chem. Eng. J. 4 (1972) 31–40.
[13] A. Schumpe, Chem. Eng. Sci. 48 (1993) 153–158.
[14] G.F. Versteeg, W.P.M. van Swaaij, J. Chem. Eng. Data 33 (1988) 29–34.
[15] A.L. Horvath, Handbook of Aqueous Electrolytic Solutions: Physical Properties, Estimation and Correlation Methods, Wiley, New York, 1985.
[16] R. Pohorecki, W. Moniuk, Chem. Eng. Sci. 43 (1988) 1677–1684.
[17] M. Eigen, Discussions Faraday Soc. 17 (1954) 194–205.
[18] T.J. Edwards, G. Maurer, J. Newman, J.M. Prausnitz, A.I.Ch.E. J. 24 (1978) 966–976.
[19] C. Tsonopoulos, J. Chem. Eng. Data 21 (1976) 190–193.
[20] B.R.W. Pinsent, F.J.W. Roughton, Trans. Faraday Soc. 47 (1951) 263–269.
[21] B.R.W. Pinsent, L. Pearson, F.J.W. Roughton, Trans. Faraday Soc. 52 (1956) 1512–1520.
[22] D.M. Himmelblau, A.L. Babb, A.I.Ch.E. J. 4 (1958) 143–152.
[23] P.V. Danckwerts, A.M. Kennedy, Chem. Eng. Sci. 8 (1958) 201–215.
[24] R.A.T.O. Nijsing, R.H. Hendriksz, H. Kramers, Chem. Eng. Sci. 10 (1959) 88–104.
[25] D. Roberts, P.V. Danckwerts, Chem. Eng. Sci. 17 (1962) 961–969.